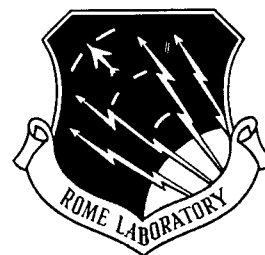


**RL-TR-97-19**  
**Final Technical Report**  
**June 1997**



# **LOW-LOSS FIBER-OPTIC TRUE TIME DELAY GENERATOR FOR RF SIGNAL PROCESSING AND PHASED ARRAY ANTENNA CONTROL (TTD)**

**TRW Space and Electronics Group**

**Michael Wickham, Larry Dozal, and John Brock**

*APPROVED FOR PUBLIC RELEASE; DISTRIBUTION UNLIMITED.*

19970728 162


DTIC QUALITY INSPECTED 4

**Rome Laboratory**  
**Air Force Materiel Command**  
**Rome, New York**

This report has been reviewed by the Rome Laboratory Public Affairs Office (PA) and is releasable to the National Technical Information Service (NTIS). At NTIS it will be releasable to the general public, including foreign nations.

RL-TR-97-19 has been reviewed and is approved for publication.

APPROVED:



DONALD LUCZAK  
Project Engineer

FOR THE COMMANDER:



DONALD W. HANSON, Director  
Surveillance & Photonics Directorate

If your address has changed or if you wish to be removed from the Rome Laboratory mailing list, or if the addressee is no longer employed by your organization, please notify RL/OCPC, 25 Electronic Pky, Rome, NY 13441-4514. This will assist us in maintaining a current mailing list.

Do not return copies of this report unless contractual obligations or notices on a specific document require that it be returned.

REPORT DOCUMENTATION PAGE			Form Approved OMB No. 0704-0188	
Public reporting burden for this collection of information is estimated to average 1 hour per response, including the time for reviewing instructions, searching existing data sources, gathering and maintaining the data needed, and completing and reviewing the collection of information. Send comments regarding this burden estimate or any other aspect of this collection of information, including suggestions for reducing this burden, to Washington Headquarters Services, Directorate for Information Operations and Reports, 1215 Jefferson Davis Highway, Suite 1204, Arlington, VA 22202-4302, and to the Office of Management and Budget, Paperwork Reduction Project (0704-0188), Washington, DC 20503.				
1. AGENCY USE ONLY (Leave blank)	2. REPORT DATE June 1997	3. REPORT TYPE AND DATES COVERED Final Nov 94 - Oct 96		
4. TITLE AND SUBTITLE  LOW-LOSS FIBER-OPTIC TRUE TIME DELAY GENERATOR FOR RF SIGNAL PROCESSING AND PHASED ARRAY ANTENNA CONTROL (TTD)		5. FUNDING NUMBERS  C - F30602-93-C-0203 PE - 62702F PR - 4600 TA - P2 WU - 11		
6. AUTHOR(S)  Michael Wickham, Larry Dozal and John Brock				
7. PERFORMING ORGANIZATION NAME(S) AND ADDRESS(ES)  TRW Space and Electronics Group Space and Technology Division One Space Park Redondo Beach CA 90278		8. PERFORMING ORGANIZATION REPORT NUMBER  N/A		
9. SPONSORING/MONITORING AGENCY NAME(S) AND ADDRESS(ES)  Rome Laboratory/OCPC 25 Electronic Pky Rome, NY 13441-4514		10. SPONSORING/MONITORING AGENCY REPORT NUMBER  RL-TR-97-19		
11. SUPPLEMENTARY NOTES  Rome Laboratory Project Engineer: Donald Luczak/OCPC/(315) 330-3144				
12a. DISTRIBUTION AVAILABILITY STATEMENT  Approved for public release; distribution unlimited		12b. DISTRIBUTION CODE		
13. ABSTRACT (Maximum 200 words)  The work established the viability of a fiber-optic approach for low-loss true time delay of wideband RF signals for phased-array antenna (PAA) beamsteering. In this approach an optical carrier modulated by the RF signal of interest is launched into a delay-line fiber composed of optical Bragg reflection gratings written holographically into the core of a single-mode fiber. The beam is steered by tuning the optical carrier wavelength for reflection from the appropriate grating. The fiber Bragg grating writing performance meets and exceeds PAA requirements. We demonstrated: 1) a time delay accuracy of approximately 2 ps (20 ps verified); 2) a wavelength writing accuracy for Bragg gratings of 0.04 nm absolute, 0.01 nm relative; 3) a sidelobe suppression of 50 dBe at 2 nm channels and 60 dBe at 3 nm channels. We produced a 4-bit, 16 grating true time delay element which includes an optical circulator. An analytical model, which includes chirp, was developed that predicts both the optical and RF response for the fiber optic Bragg grating.				
14. SUBJECT TERMS  True Time Delay, Phased-Array Antennas (PAA), Bragg Gratings		15. NUMBER OF PAGES 60		
		16. PRICE CODE		
17. SECURITY CLASSIFICATION OF REPORT  UNCLASSIFIED	18. SECURITY CLASSIFICATION OF THIS PAGE  UNCLASSIFIED	19. SECURITY CLASSIFICATION OF ABSTRACT  UNCLASSIFIED	20. LIMITATION OF ABSTRACT  SAR	

## Table of Contents

List of figures.....	ii
List of Tables.....	v
1.0 Introduction .....	1
2.0 Theoretical Modeling.....	8
3.0 Grating Writing Facility .....	16
4.0 Experimental Results.....	20
5.0 True Time Delay Deliverable .....	31
6.0 Planar Silica Waveguides and Hydrogen Loading .....	40
7.0 Conclusions .....	46

## List of Figures

Figure 1-1. Transmission spectrum of the True Time Delay deliverable fiber with 16 gratings. Envelope follows LED spectrum used for the measurement.....	2
Figure 1-2. The Bragg grating True Time Delay element is a low loss device that selects the delay of RF signal by tuning the optical carrier wavelength.....	3
Figure 1-3. Optical pulses reflected off the 16 Bragg gratings written at 16 wavelengths for the True Time Delay deliverable.....	4
Figure 1-4. The fiber optic Bragg grating time delay technique lends itself to wavelength controlled beamsteering and signal multiplexing.....	6
Figure 1-5. Gratings may be positioned within the fibers to compensate for nonplanar radiating surfaces if needed. This is the optical equivalent of an RF Rotman lens.....	7
Figure 2-1. Theoretical optical response for three grating profiles with channel isolation figures shown at 38 dB <sub>e</sub> and 86 dB <sub>e</sub> .....	9
Figure 2-2. Theoretical writing profiles for the sharp half gaussian and the tapered gaussian profiles.....	10
Figure 2-3. Reflectivity spectrums for the sharp half gaussian and the tapered gaussian profiles.....	10
Figure 2-4. Channel isolation vs. number of channel in a 50 nm bandwidth.....	11
Figure 2-5. The optical response of weak and strong gratings shows a flat response over the useful portion of the gratings. The higher reflectivity of the strong gratings come at the expense of higher bandwidth and thus reduced channel isolation.....	12
Figure 2-6. The RF response of weak and strong gratings has a flat phase response over the useful portion of the gratings.....	13
Figure 2-7. Theoretical optical response for grating with three different chirps...	14
Figure 2-8. Theoretical optical phase and magnitude for a grating with linear chirp.....	14
Figure 2-9. Measured grating profile with the theoretically predicted profile for gaussian chirp. AT&T Accutether 220 type fiber used here.....	15

Figure 3-1. TRW capitol grating writing facility.....	17
Figure 3-2. TRW grating writing facility with new Far field camera.....	18
Figure 4-1. R=84% Bragg fiber grating transmission spectra of Andrews Series E polarization preserving fiber.....	21
Figure 4-2. Optical reflectivity spectrum of a) Spectran b) AT&T Accutether 220 and c) AT&T dispersion compensating fiber.....	22
Figure 4-3. Reflectivity vs. Time for Andrews Series E finer and AT&T Accutether 220 single mode fiber.....	23
Figure 4-4. Grating center wavelength shift vs. Tension. The slope is 0.013 nm/gm for the Accutether 220 type fiber.....	24
Figure 4-5. Half Gaussian and new "soft" modeled grating writing intensity profiles.....	25
Figure 4-6. Reflectivity profile for the old half gaussian and new "soft" gratings.....	26
Figure 4-7. Channel isolation vs. channel width for half gaussian and "soft" gratings.....	26
Figure 4-8. Fiber grating RF characterization test diagram.....	27
Figure 4-9. RF phase measured from 0.303.0 GHz. The laser was tuned to the center frequency of the Bragg grating,.....	28
Figure 4-10. Time delay measurement apparatus.....	29
Figure 4-11. Measured time delay pulses from 4 equally spaced gratings.....	30
Figure 5-1. True Time Delay deliverable. Dimensions are in inches and there is a APC connector union at the fiber (not shown) to facilitate the exchange of the grating fiber.....	31
Figure 5-2. True time delay package size with Optics for Researches circulator (right) and the new JDS Fitel circulator (left).....	32
Figure 5-3. Transmission spectrum of 16 grating fiber. Gratings were written in AT&T Accutether 220 fiber.....	33
Figure 5-4. Measured reflectivity for each grating.....	33

Figure 5-5. Reflectivity spectrum of grating written in Accutether 220 showing main reflectivity peak at 1308 nm and secondary reflectivity peak at 1305 nm...	35
Figure 5-6. Reflectivity spectrum of grating written in AT&T's Dispersion compensating fiber at 1326 nm.....	35
Figure 5-7. Transmission spectra of 16 grating fiber.....	37
Figure 5-8. Measured reflectivity for each grating.....	37
Figure 5-9. Time delayed pulses from the 16 grating True Time Delay deliverable.....	39
Figure 5-10. Time delay vs. Grating number and linear fit to the data.....	39
Figure 6-1. Silica planar waveguide structure purchased from PIRI.....	40
Figure 6-2. Hydrogen loading cell.....	42
Figure 6-3. Transmission spectrum of the hydrogen loaded planar silica waveguide material after 2 Bragg gratings were written in one of the channels.....	43
Figure 6-4. Transmission spectrum of a single channel after 4 minute of exposure to UV.....	43
Figure 6-5. Transmission spectrum of a single channel after 8 minutes of exposure.....	44
Figure 6-6. Transmission spectrum of Hydrogen loaded AT&T Dispersion Compensation Fiber after 10 seconds of exposure to a 11 mW 244 nm beam..	45
Figure 6-7. Transmission spectrum of Hydrogen loaded AT&T Dispersion Compensation Fiber after 11 minutes of exposure to a 11 mW 244 nm beam...	45

## **List of Tables**

Table 4-1. Fiber types used in the True Time Delay Program.....	20
Table 5-1. Measured parameters of the first 16 grating.....	34
Table 5-2. 16 grating measured parameters.....	38
Table 5-3. Center wavelength positions and peak reflectivity for the 16 gratings in the True Time Delay deliverable.....	38



## 1.0 Introduction

The True Time Delay program (Low-Loss Fiber-Optic True Time Delay Generator for RF Signal Processing and Phased Array Antenna Control) has, over the last three years, developed the fiber optic Bragg grating True Time Delay concept to a form that could be implemented into a phased array system. In addition, the True Time Delay program has positioned us to develop a wide class of RF photonic signal processing structures.

During the course of the program we have proven our ability to make high quality fiber optic Bragg gratings, the key element in the fiber optic Bragg grating True Time Delay concept. We have:

- written gratings in 5 different types of fiber that are single mode at  $1.3\mu\text{m}$  and  $1.5\mu\text{m}$  with reflectivity's as high as 99% without hydrogen loading;
- developed the ability to write gratings in planar silica waveguide material;
- achieved sidelobe suppression of 50 dBe at 2 nm channels and 60 dBe at 3 nm channel spacing;
- written gratings in polarization preserving fiber and non polarization preserving fibers;
- developed an analytical model to predict the performance characteristics of the gratings for any chirp and grating writing intensity profile;
- demonstrated high precision wavelength positioning of 0.036 nm absolute and 0.01 nm relative;
- developed a system for high spatial positioning accuracy, which translates to time delay accuracy of 2-3 picosecond, with 28 picosecond verified;
- designed and fabricated a TTD element that contains a 16 grating, 4-bit, time delay element with an optical circulator.

Data taken with the deliverable TTD element is shown in Figure 1-1. The transmission spectrum shows the transmission dips of the 16 gratings. The envelope of the transmission curve follows the spectral shape of the LED used to perform the measurement. This data is presented more completely later in section 5.0,.

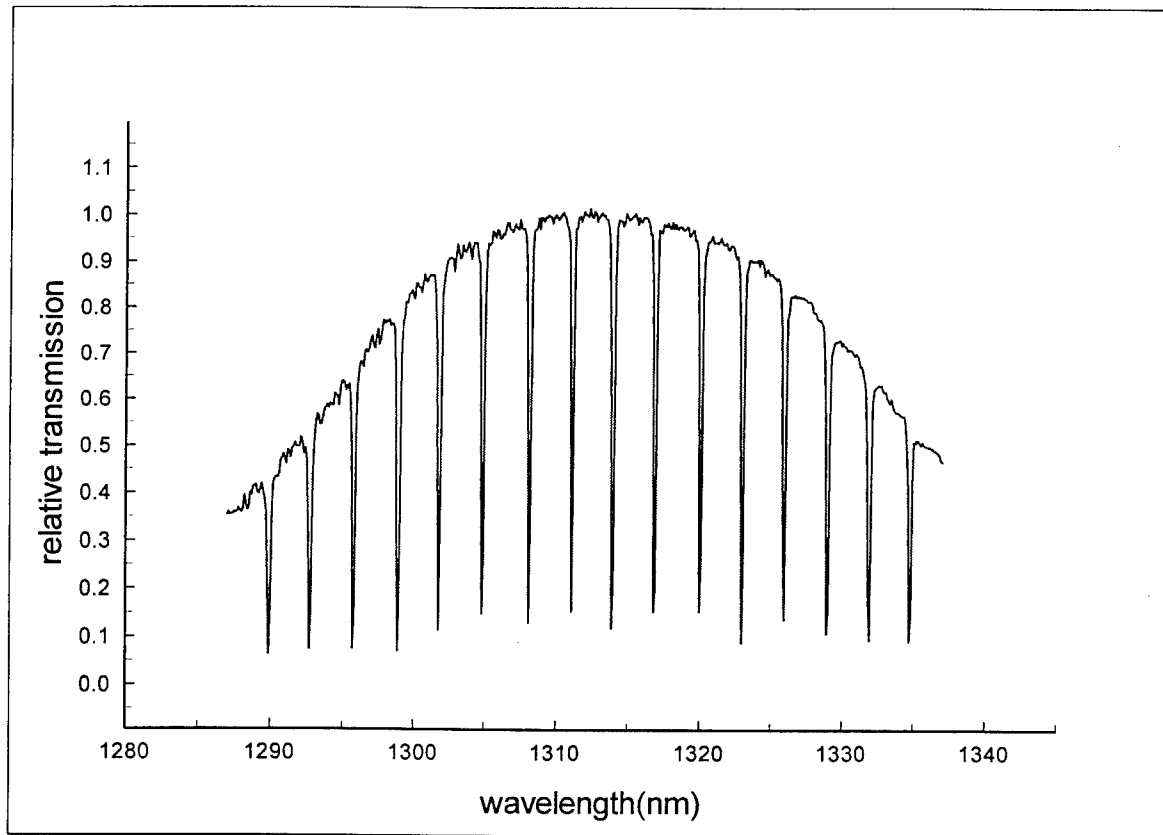


Figure 1-1. Transmission spectrum of the True Time Delay deliverable fiber with 16 gratings. Envelope follows LED spectrum used for the measurement.

The motivation for this current effort has been the performance improvement that True Time Delay allows for phased array antennas (PAAs). Beam squint is the most significant bandwidth limiting effect in PAAs that require wide-angle scanning. To limit the effects of beam squint, broadband phased-array antennas (PAAs) require true-time delay (TTD) devices positioned at each antenna subarray. Conventional RF phased array antennas achieve true-time delay by using switching systems that select different lengths of cable or waveguide sections according to the required time delay. RF delay lines capable of providing delays of these lengths usually have unacceptably high attenuation losses and are bulky and heavy. These limitations can be surmounted by photonic RF time delay generators where the RF signal is impressed on an optical carrier that can be delayed in relatively low loss fiber optic cabling. In general,

therefore, establishing a need for true-time delay can be a powerful argument for the use of an optical feed network.

Most optical implementations of true-time delay consist of switching into place various lengths of fiber-optic cable and/or waveguide. The differences among the various methods consist mainly in the method by which the switching takes place. Such optical switching matrices have several disadvantages. They have significant insertion loss, they require active electrical control signals with the associated drive leads, electronics, and power consumption, and they can be physically bulky. Moreover, optical crosstalk in the switches can be a limiting factor in total system dynamic range.

Figure 1-2 illustrates the Bragg grating true-time delay concept which alleviates the RF insertion loss and complexity associated with other switching approaches<sup>1,2</sup>. A series of Bragg reflection gratings have been holographically written into the core of a single-mode fiber at different positions. Each grating reflects only a narrow frequency band of light, i.e., grating #1 reflects  $\lambda_1$ , grating #2 reflects  $\lambda_2$ , etc. Different time delays are selected by tuning the optical carrier to the wavelength that matches the appropriate reflection grating.

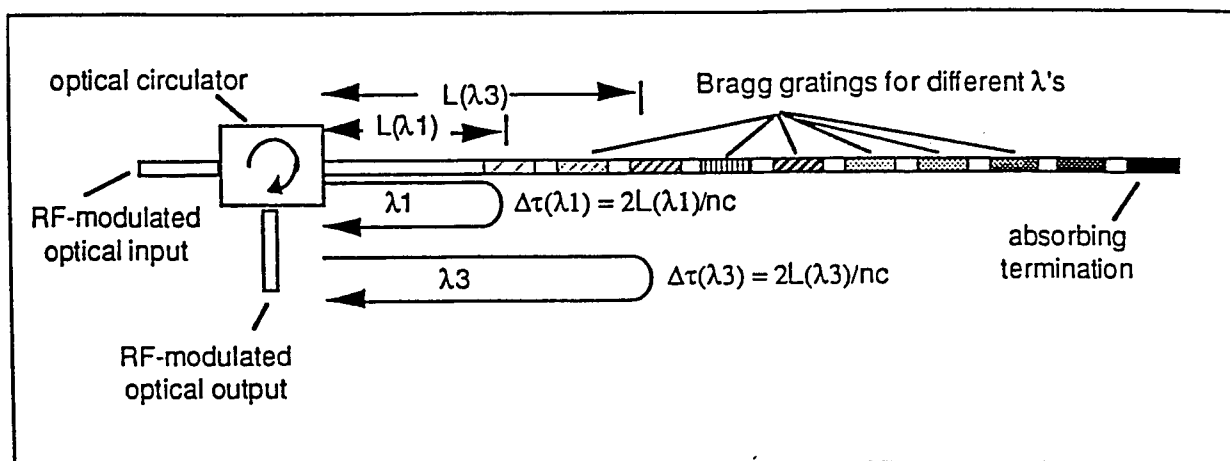


Figure 1-2. The Bragg grating True Time Delay element is a low loss device that selects the delay of RF signal by tuning the optical carrier wavelength.

Gratings with reflectivity exceeding 90% can be routinely produced; relative time delay resolutions of  $<10$  psec are also possible. In Figure 1-3 is shown data taken with the True Time Delay element with 16 gratings written at 16 different wavelengths. The separation of each grating was controlled to an accuracy of  $25\text{ }\mu\text{m}$  or a time delay accuracy of 2.5 ps. The time resolution, 20 ps, in this case was limited by the modulator used to create the optical pulses.

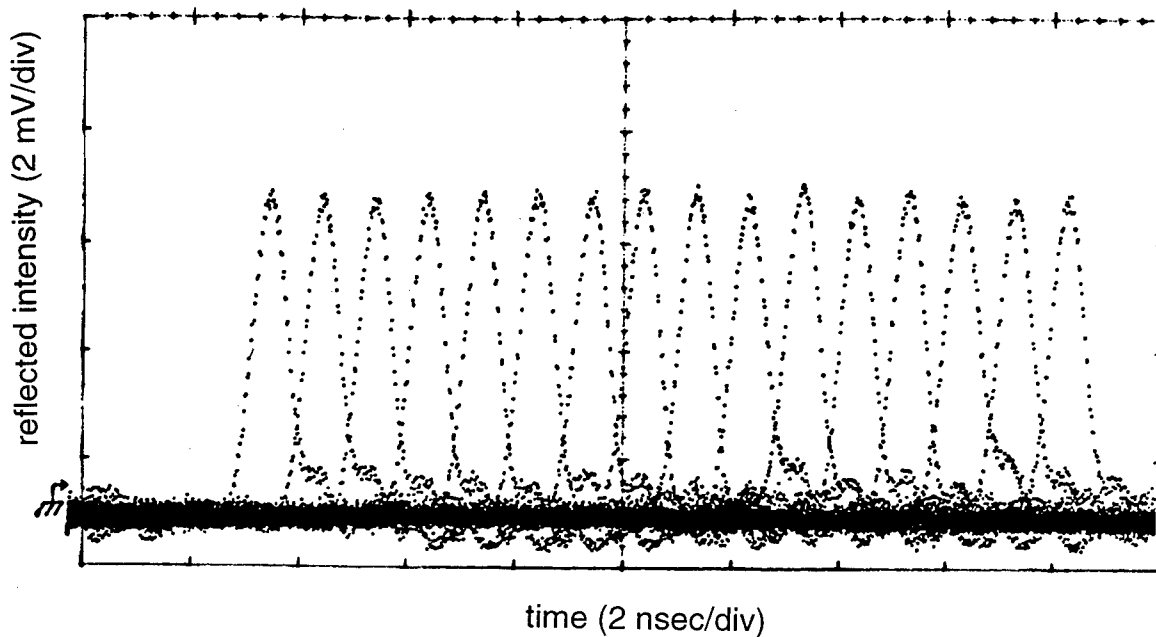


Figure 1-3. Optical pulses reflected off the 16 Bragg gratings written at 16 wavelengths for the True Time Delay deliverable.

Since the Bragg gratings are nearly lossless in transmission outside their reflection bandwidth, many time delays can be contained within a single length of optical fiber, and addressed through a single input/output coupler, making the RF insertion loss of the time-delay element virtually independent of the number of time delays. A 10% optical loss (due to a 90% reflection grating) would contribute 1 dB to the RF insertion loss of the device. Optical circulators having a round-trip optical insertion loss of  $< 2$  dB, or an RF insertion loss of  $< 4$  dB, are now commercially

available. We thus expect less than 5 dB of RF insertion loss from this device, almost independently of the time-delay bit resolution. A second major advantage to the wavelength-controlled time delay approach is that it lends itself to simplified beam forming technique.

### **Beam forming Networks**

A phased-array antenna must include a control subsystem to distribute time-delay, phase, and amplitude weights to each element to perform beam steering, beamwidth control, and possibly null positioning. The methods by which the control subsystem generates and distributes the appropriate weights may be described as falling somewhere between two extremes. In the first, a network is used to distribute control data to these the time delay units, phase shifters, and attenuators; a conventional control network may require several control lines for each antenna element, raising the concerns of front-end congestion and electrical interference. Alternatively, phase and amplitude control may be implemented without the need for variable phase shifters through the use of more elegant beam forming techniques such as Butler matrices or bootlace (e.g., Rotman) lenses to distribute phase programs or time-delay programs, respectively. In these devices, the signal to be radiated is switched into one of a set of input ports; each of these beam former inputs is mapped to the radiating elements by the appropriate set of path lengths to generate the desired wavefront. As presently implemented using RF techniques, both Butler matrices and bootlace lenses tend to be bulky and have high RF losses. Photonic implementations show potential for reducing the size, weight, and insertion losses of these beam formers.

The Bragg-grating time delay technique lends itself to the implementation of one such beam forming technique in an optically fed PAA, using optical wavelength as the control variable. This technique is shown in Figure 1-4, which illustrates the relative placement of time-delay gratings within the optical delay fibers for two different

subarrays of a transmit-mode antenna. The time-delay selected by a given optical wavelength differs for each subarray, such that each wavelength corresponds to a particular beam direction. As illustrated in Figure 1-5, gratings may be positioned within the fibers to compensate for nonplanar radiating surfaces if needed. This technique may be viewed as the optical equivalent of an RF Rotman lens: wavelength tuning serves the same function as electronic signal routing to the appropriate input port of the Rotman lens. The number of optical wavelengths required for this scheme is equal to the number of required beam directions. In addition, this method allows multi-channel operation by wavelength-division-multiplexing of various RF signals, using the same time-delay hardware. One simply chooses the optical carrier wavelength of a given RF wavelength according to the desired beam direction.

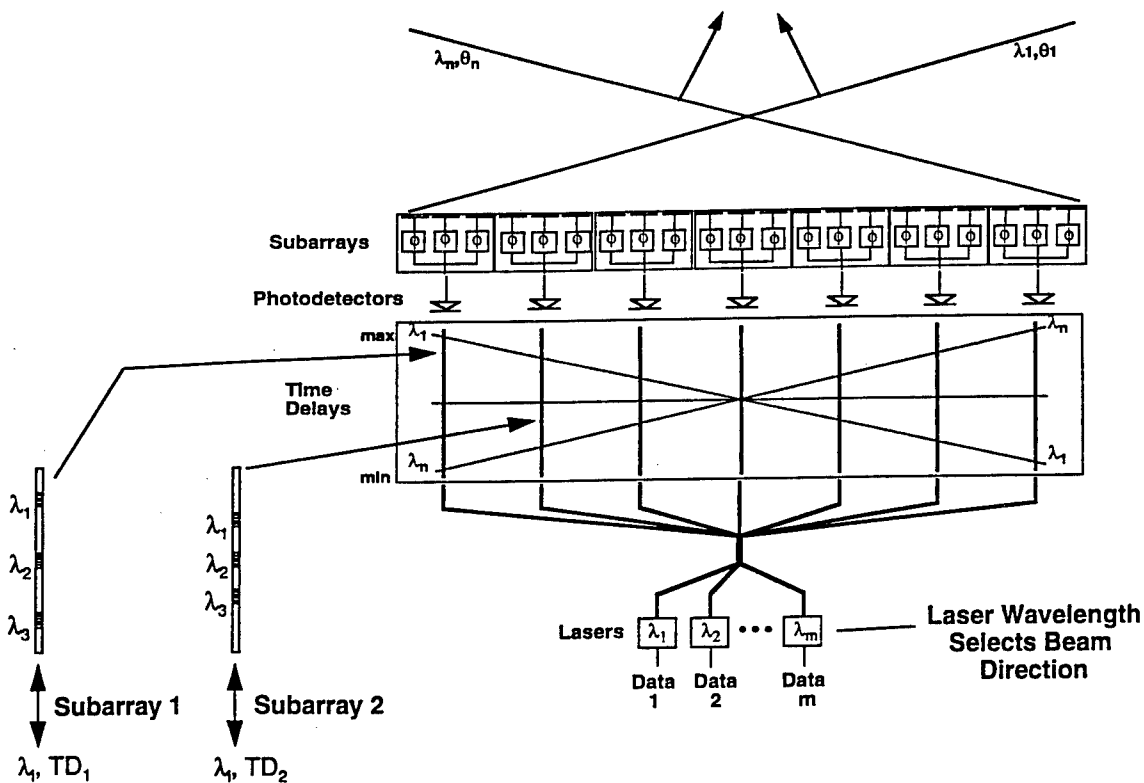


Figure 1-4. The fiber optic Bragg grating time delay technique lends itself to wavelength controlled beamsteering and signal multiplexing.

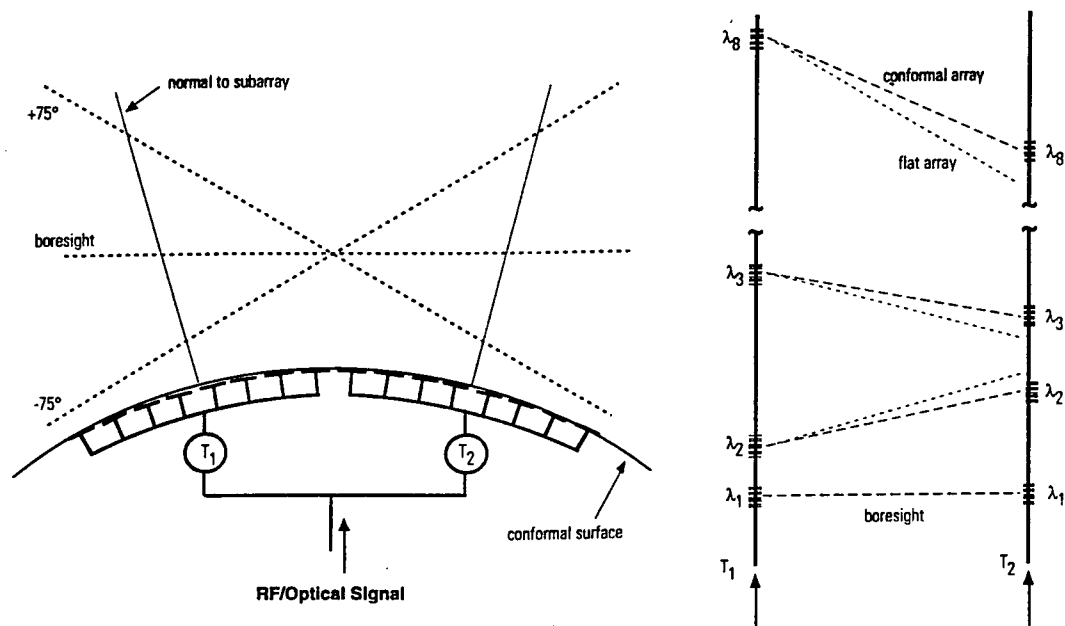


Figure 1-5. Gratings may be positioned within the fibers to compensate for nonplanar radiating surfaces if needed. This is the optical equivalent of an RF Rotman lens.

## 2.0 Theoretical Modeling

The modeling effort that was started under TRW IR&D has continued and expanded to include True Time Delay interests. The optical reflectivity spectrum and the RF response to it are calculated for various writing intensity profiles. The theoretical modeling follows the treatment by Kogelnik<sup>1 2</sup>. The model is a coupled wave analysis for the diffraction of light by a thick hologram and is valid even for large diffraction efficiencies where the incident wave is strongly depleted. The theory can be applied to both transmission and reflection holograms. Chirp and non normal fringes are allowed. The solution reduces to the solution of the Riccati equation which is solved numerically

$$\frac{d\rho}{dz} = j(2\delta - \frac{d\Phi}{dz})\rho + j\kappa(1 + \rho^2), \quad \rho = \frac{S}{R} e^{-j\Phi}$$

S and R are the forward and reverse amplitudes, the optical intensity reflectivity is  $\rho \rho^*$ . Chirp is introduced via the  $d\Phi/dz$  term and the wavelength or frequency detuning from the Bragg condition is represented by  $\delta$ .  $\delta = 0$  is the center or Bragg condition. The equation is separated into its real and imaginary parts. Those two coupled nonlinear equations are then solved numerically on a PC using the commercial software MathCad 6\* for each desired value of  $\delta$ . To calculate an entire reflectivity spectrum the equations must be solved many times depending on the desired resolution of the spectrum. The RF response,  $G_{RF}$ , is related to the optical response of the grating,  $\rho$ , by the relation below:

$$G_{RF}(\omega_{RF}, \omega_{opt}) = \rho^*(\omega_{opt})\rho(\omega_{opt} + \omega_{RF}) + \rho(\omega_{opt})\rho^*(\omega_{opt} - \omega_{RF})$$

$\rho^*$  is the complex conjugate of  $\rho$ . After calculating the optical response,  $\rho(\omega_{opt})$ , the RF response is calculated.

---

<sup>1</sup>Herwig Kogelnik, "Coupled Wave Theory for Thick Hologram Gratings", The Bell Systems Technical Journal V48 Nov 1969, Number 9

<sup>2</sup>H. Kogelnik, " Filter Response of Nonuniform Almost-Periodic Structure", The Bell Systems Technical Journal, V.55, Jan 1976, No. 1



The theoretical optical response of three grating profiles is shown in Figure 2-1. The shapes of the profiles, shown in the figure, are full and half gaussian as well as a flat top profile. The grating writing intensity profile is important for maximizing time delay channel isolation.

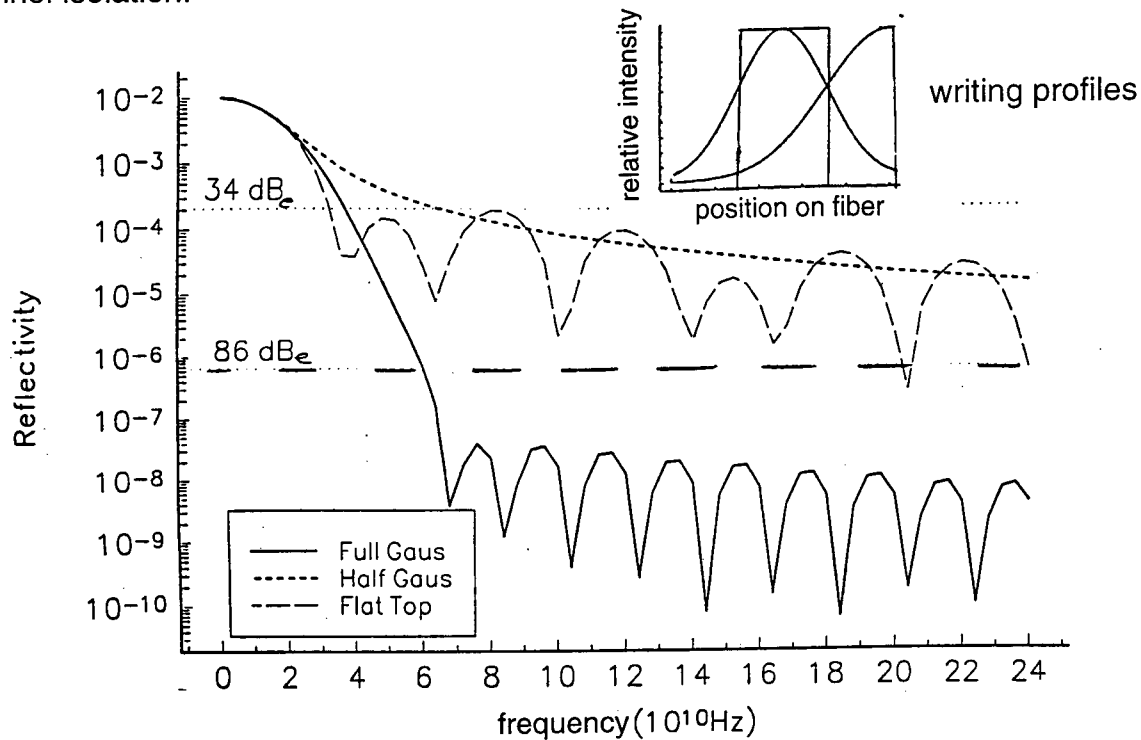


Figure 2-1. Theoretical optical response for three grating profiles with channel isolation figures shown at 34 dB<sub>e</sub> and 86 dB<sub>e</sub>. Insert shows intensity writing profiles.

The half gaussian profile, which is the profile resulting from a common grating producing geometry using a prism, will produce a half gaussian profile with inferior channel isolation compared to the full gaussian. The prism technique can produce a gaussian like profile when the cylindrical lens is adjusted so that the line focus is not collinear to the fiber core. The writing profile of the sharp half gaussian and the soft gaussian like profiles are shown in Figure 2-2. The corresponding theoretical reflectivity profiles are shown in Figure 2-3. While the soft gaussian has a wider FWHM, it falls off much faster allowing a closer adjacent grating placement. The importance of the

reflectivity spectrum due to the soft gaussian can be seen in Figure 2-4 when one plots the channel isolation vs., number of channel that can be fit into 50 nm. The tapered gaussian has much better channel isolation. Gratings were written with this technique and the results are shown in section 4.0 Experimental Results.

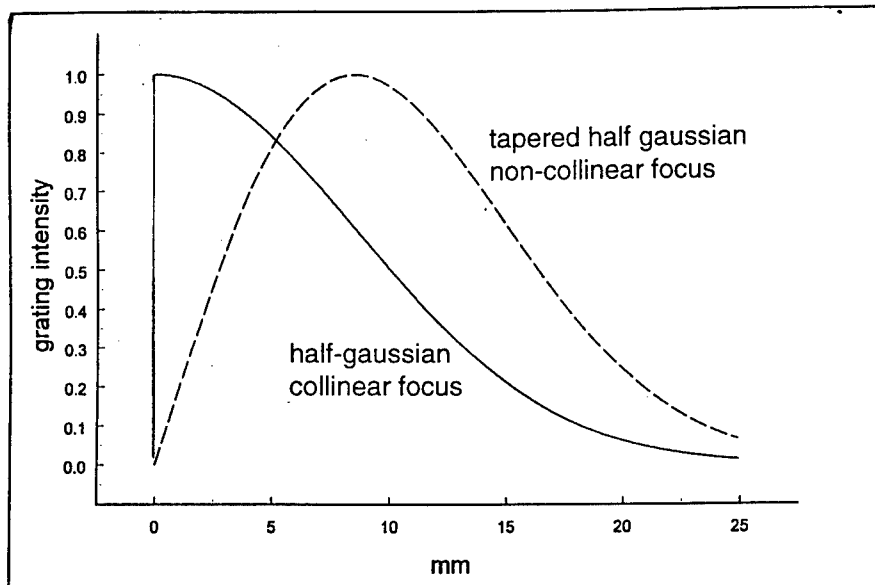


Figure 2-2. Theoretical writing profiles for the sharp half gaussian and the tapered gaussian profiles.

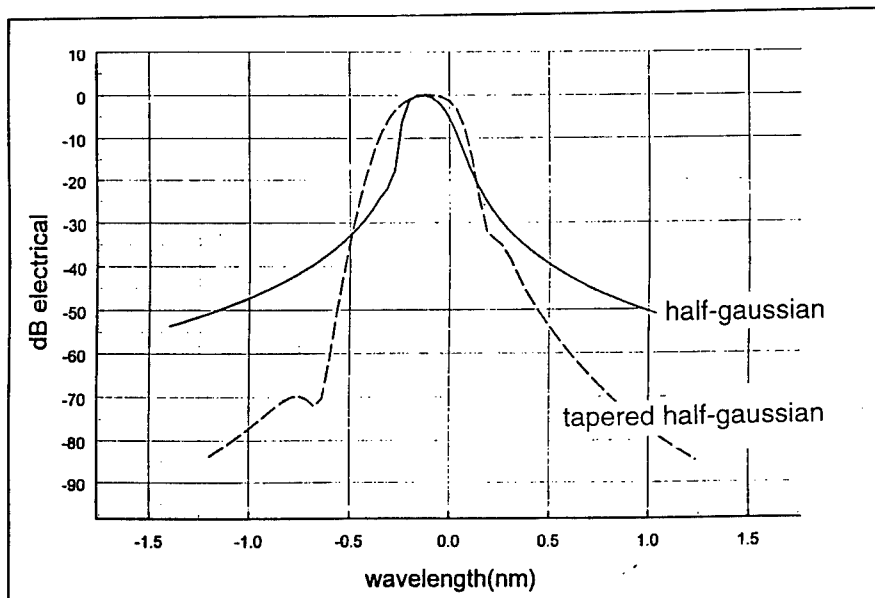


Figure 2-3. Reflectivity spectra for the sharp half gaussian and the tapered gaussian profiles.

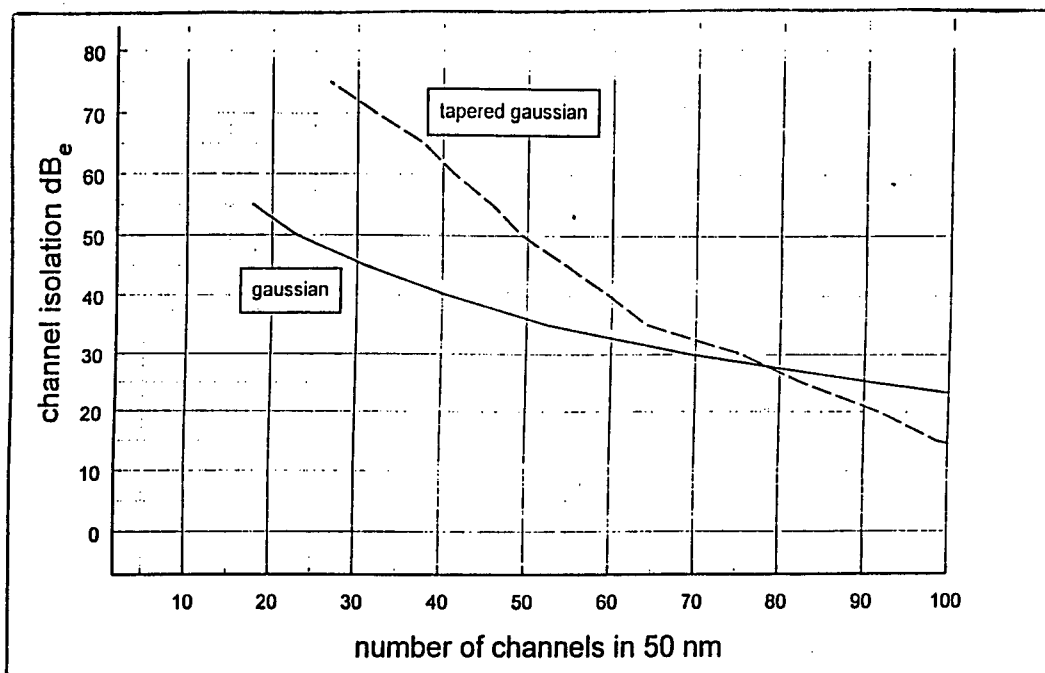


Figure 2-4. Channel isolation vs. number of channel in a 50 nm tuning bandwidth of the optical carrier source.

The optical reflectivity and phase response of a grating written with a half gaussian profile is shown in Figures 2-5 a) and b). The response is shown for a weak (10% reflectivity) and a strong grating. As long as the optical carrier wavelength is within the full width half maximum of the grating bandwidth, then the phase error of the RF response will be less than 4 degrees. RF amplitude equalization is then the driving issue not phase errors. Figure 2-6 shows that the phase response is linear over a large RF bandwidth.

Chirp arises due to a mean index variation along the grating profile which arises from the grating writing intensity profile. To make the model complete, chirp was added. As the mean index varies, so does the Bragg wavelength. The Bragg wavelength is given by  $\lambda_B = 2n\Lambda$ , where  $\Lambda$  is the grating spacing in the fiber. The mean index change has been measured by noting the shift in the center wavelength and found to be  $\delta n/n = 2.8 \times 10^{-4}$ . This is a function of the optical intensity, and since optical intensity varies with spatial position, there is a chirp introduced particularly for a strong grating.

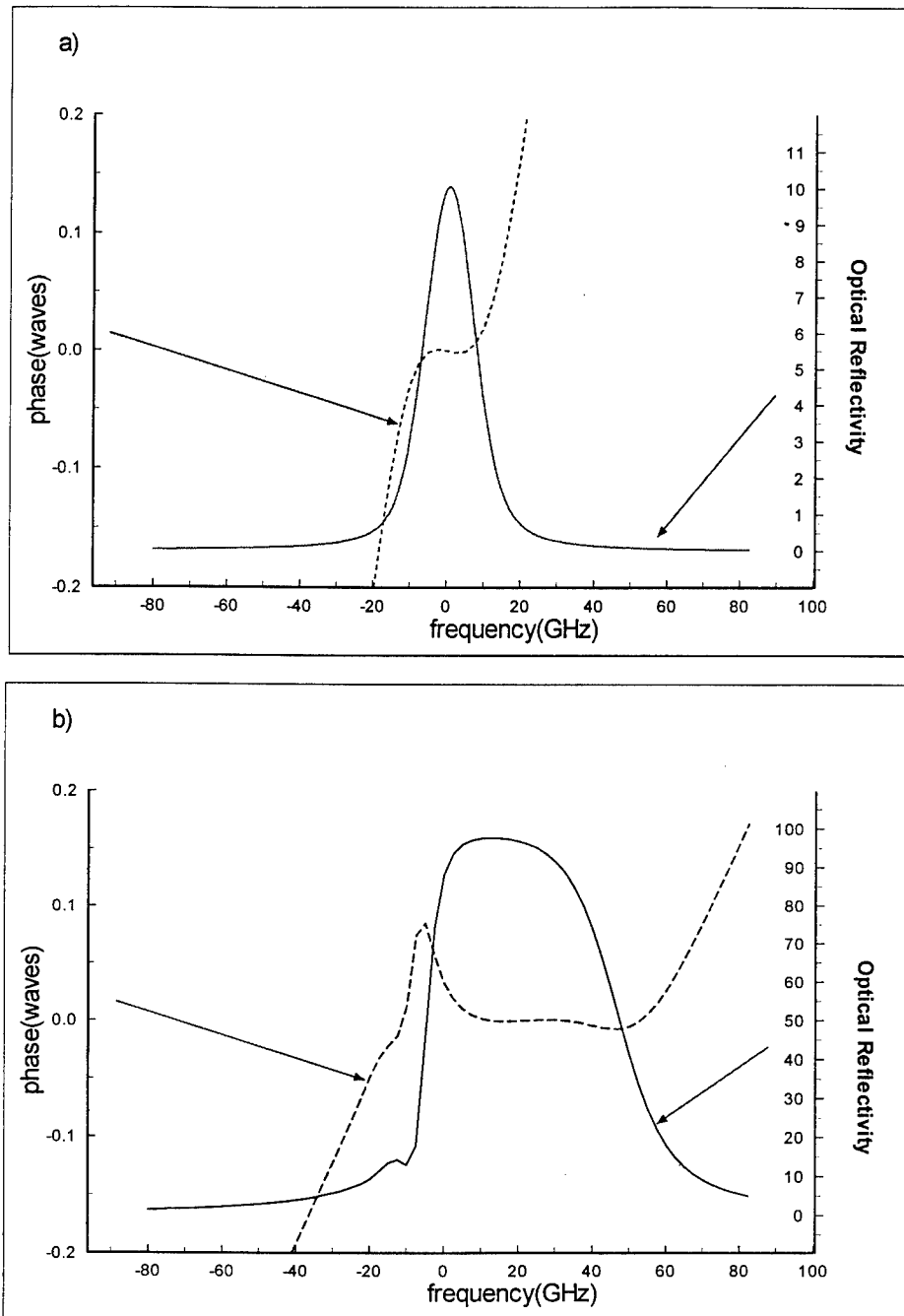


Figure 2-5. The optical response of weak a) and strong b) gratings shows a flat response over the useful portion of the gratings. The higher reflectivity of the strong gratings come at the expense of wide bandwidth and thus reduced channel isolation. The asymmetry of the strong grating is due to the grating chirp.

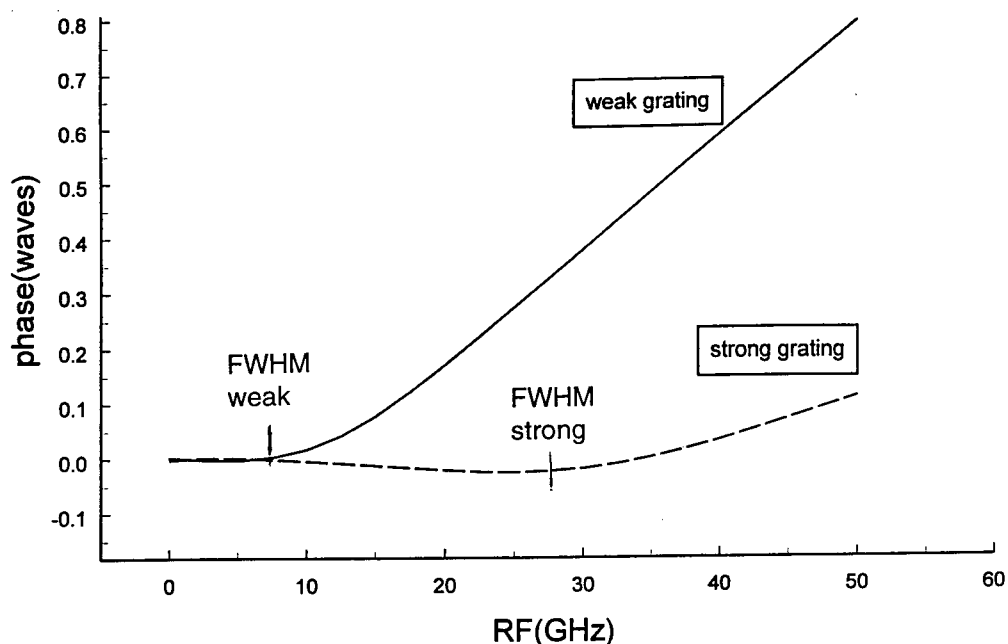


Figure 2-6. The RF response of weak and strong gratings has a flat phase response over the useful portion of the gratings.

In Figure 2-7 is shown the optical response for gratings that have several values of linear chirp. Note that the bandwidth is not significantly broadened when chirp is included but an asymmetry is evident. In Figure 2-8 is shown the optical phase along with the magnitude of the optical response for a grating with linear chirp. Note that the asymmetry is evident in the phase as well as the reflectivity.

Eggleton et al<sup>3</sup> has presented a theory to describe the chirp that is expected for grating written with a half gaussian profile, specifically for the prism method of grating writing. This information has been incorporated into our model and in Figure 2-9 is shown a measured grating profile with the theoretically predicted profile. The small scale structure in the profile is due to a hard aperture of one side of the profile of the writing intensity distribution which is slightly clipped when writing gratings at 1550 nm.

<sup>3</sup>B. Eggleton, P. Krug, L. Poladian, K.A. Ahmed and H.F. Liu, "Experimental demonstration of compression of dispersed optical pulses by reflection from self-chirped optical fiber Bragg gratings", Optics Letters, Vol.19, No.12, pg 877, 1994.

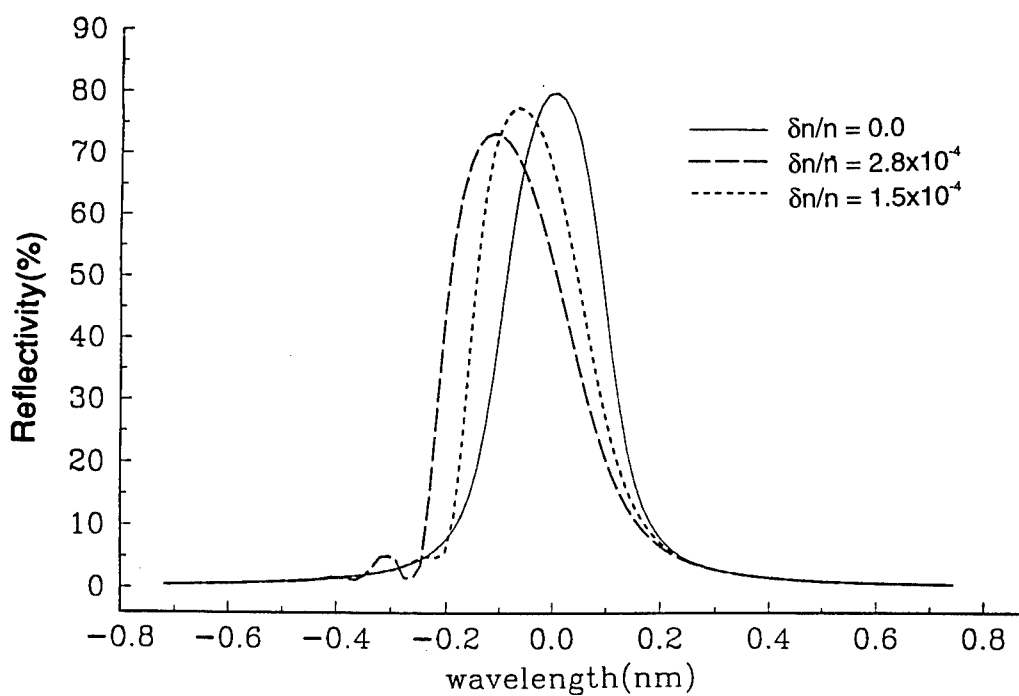


Figure 2-7. Theoretical optical response for grating with three different chirps.

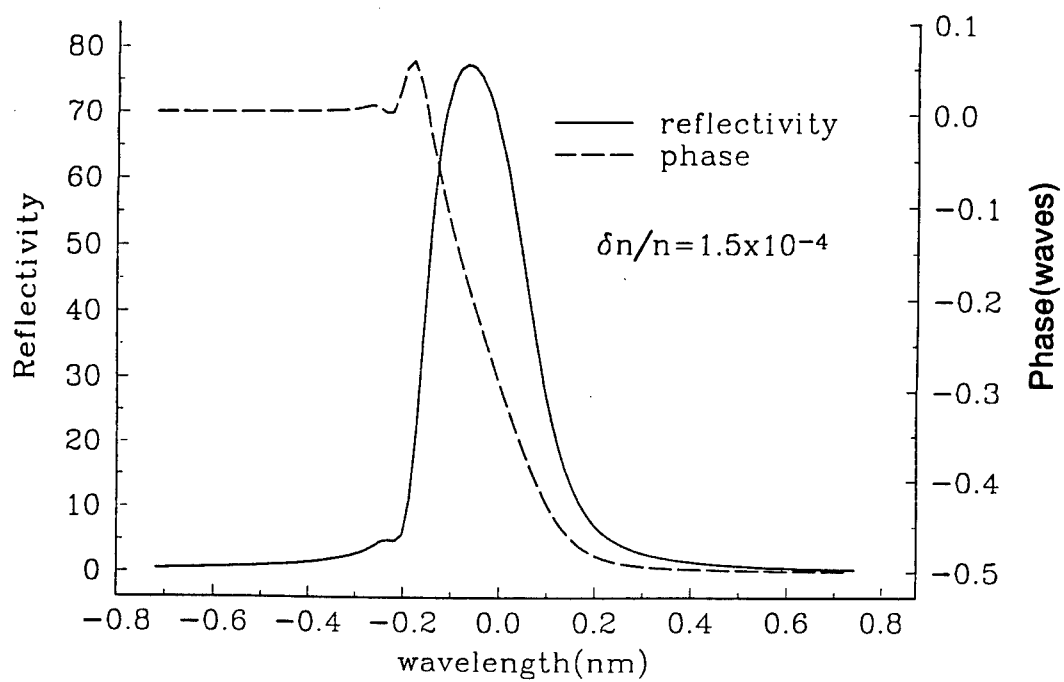


Figure 2-8. Theoretical optical phase and magnitude for a grating with linear chirp.

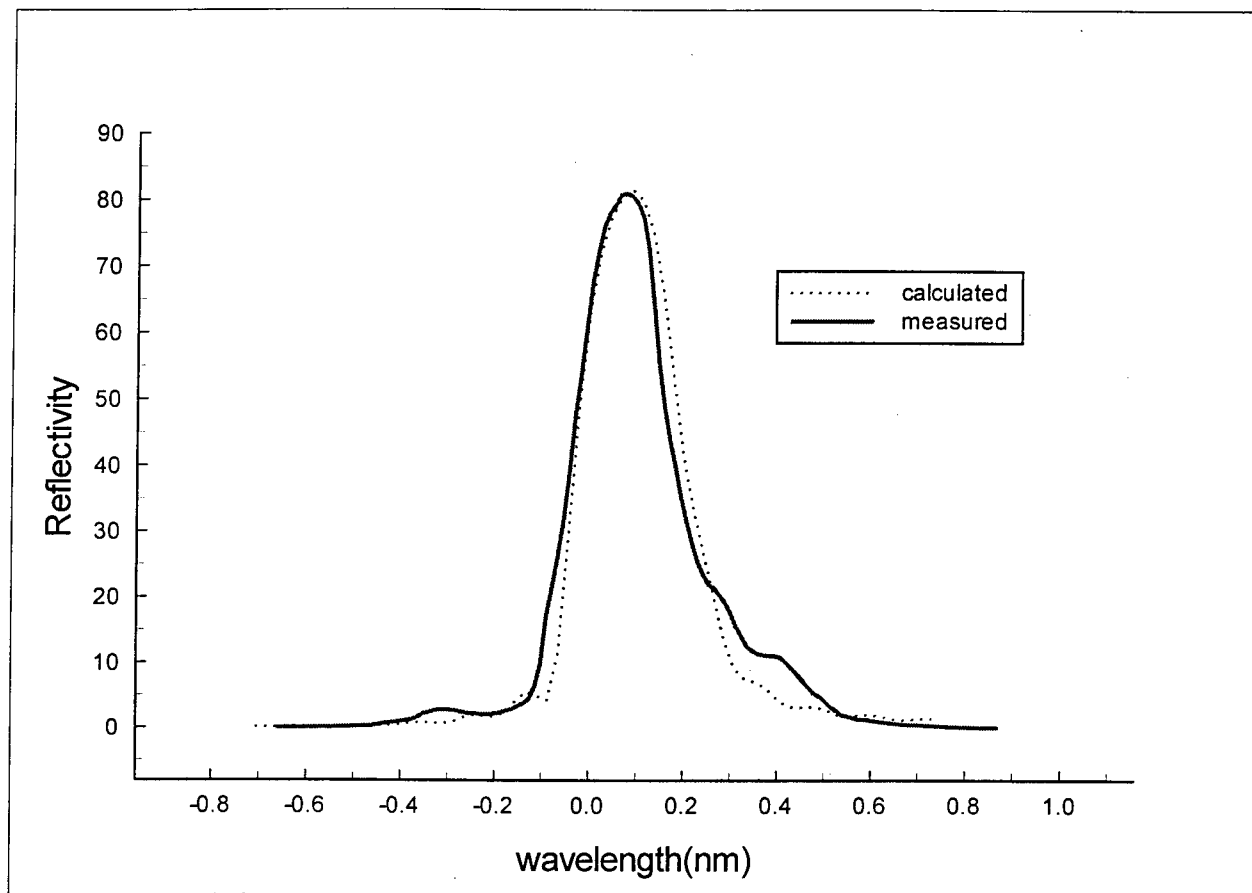


Figure 2-9. Measured grating profile with the theoretically predicted profile for gaussian chirp. AT&T Accutether 220 type fiber used here.

### 3.0 Grating Writing Facility

The grating writing facility was funded with TRW capitol and has been crucial to the success of the True Time Delay program. The main component of the facility is the UV laser, made by Coherent Corporation and was operational on January 28, 1994. The CW laser is an Argon ion laser that has a BBO crystal internal to the laser cavity and provides the frequency doubled output. The laser produces a 100 mW CW beam at 244 nm with long coherence length and excellent beam quality. This is really the key to making excellent quality fiber optic Bragg gratings. The laser and the rest of the components of the facility are shown in Figure 3-1. After exiting the laser, the beam passes through a waveplate to rotate the polarization 90°. This is necessary for correct high fringe frequency pattern to be formed. The beam is expanded with a galilean telescope and then brought to a line focus through a 2 inch prism with a cylindrical lens. Half of the beam travels directly through the prism and the other half is reflected internally off the face of the prism. The cylindrical lens must also be rotated about the beam axis to align the fiber and the line focus. The prism is mounted on a computer controlled rotation stage which can make precise rotations of the prism to change the Bragg wavelength. The CCD camera shown in the figure is used during alignment to center the focus on the fiber core. The core fluoresces visible blue light and finding the position of maximum florescence assures that the fiber is in the correct position. The fiber is held under tension on a 3 axis translation stage which has 1 micron adjustment resolution. The fiber core diameter is as small as 2 to 5 microns so this level of adjustment is required. Before mounting the fiber the buffer is removed with a mechanical stripper. The first grating for this program was written on a polarization preserving fiber made by the Andrews Corporation and was written at 1.3 micron.



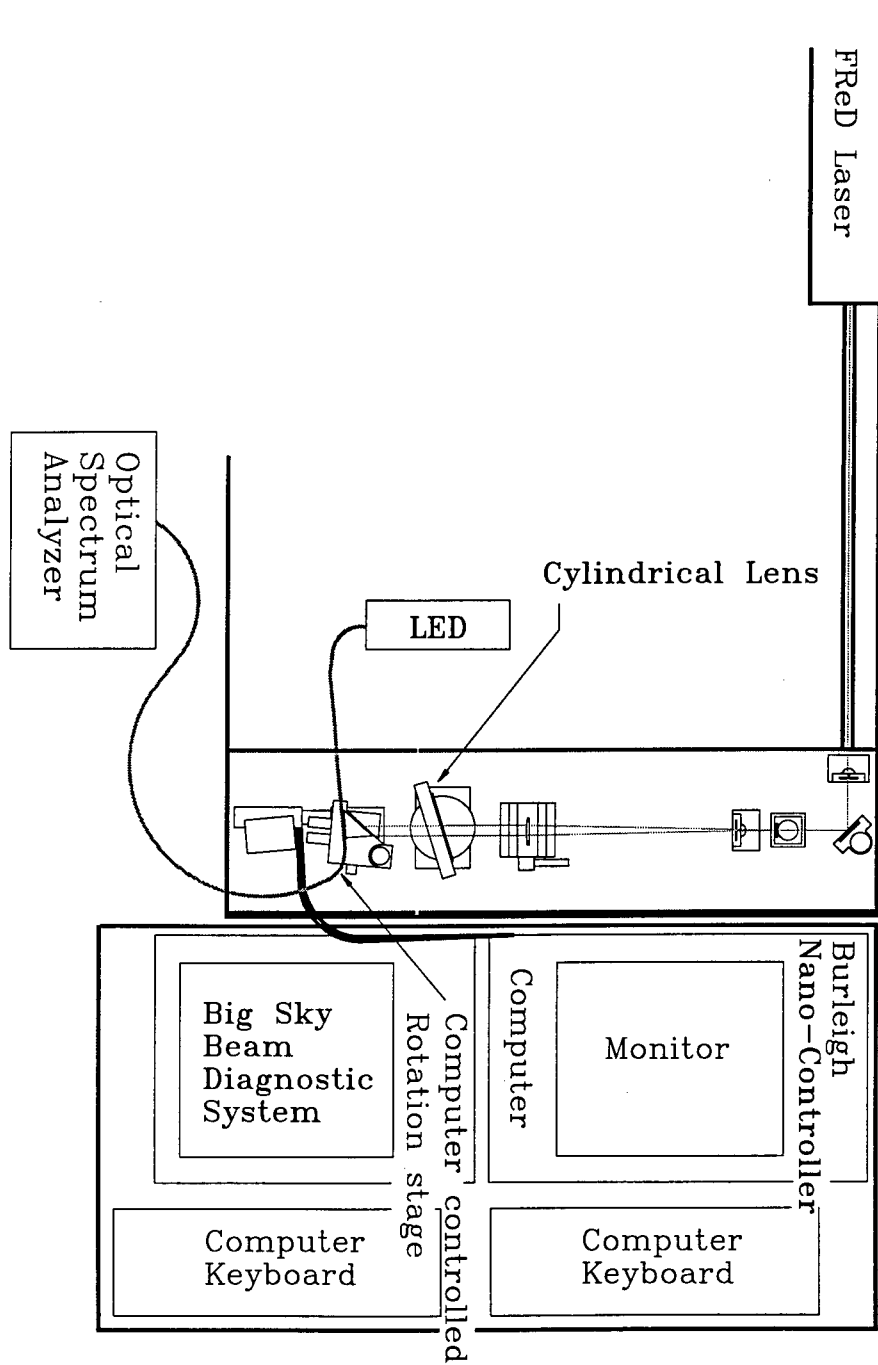


Figure 3-1. TRW capitol grating writing facility.

The ability to write gratings at the wavelength that we choose allows us to efficiently pack gratings over the useful optical tuning range of any given optical carrier source. To this end a far field camera was added to the grating writing facility, which accurately measures the prism rotation angle. There is a one to one correspondence between this angle and the grating center wavelength. The portion of the UV writing beam that is reflected off the prism is brought to focus with a 1 meter focal length lens onto a CCD camera. By using the far field camera we can now position the grating center wavelength absolutely to an accuracy better than 0.036 nm. The far field camera system can see 18.5 nm of tuning range without moving the camera. Beyond that range the CCD camera has to be moved. This can be done without losing calibration by knowing the exact wavelength before the CCD camera is moved. We have also shown that we can repeat the wavelength that we write gratings to an accuracy of 0.01 nm. A diagram of the TTD grating writing facility with the new far field camera is shown below in Figure 3-2.

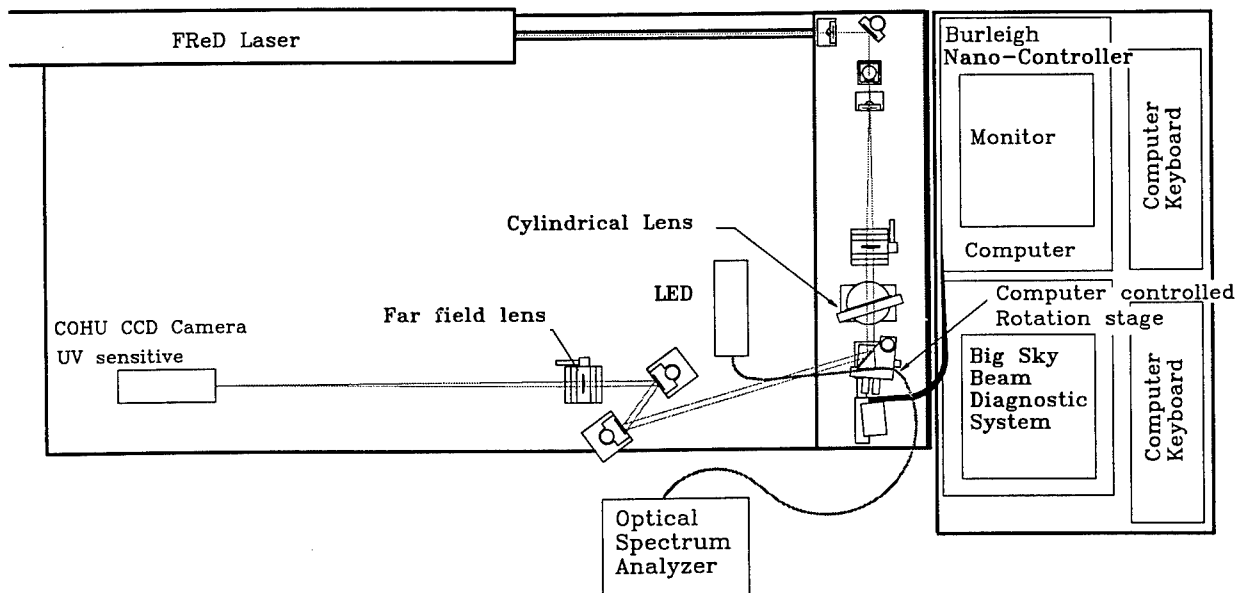


Figure 3-2. TRW grating writing facility with new Far field camera

One of the key parameters to control in the TTD application is the time delay itself. The precision that we can make time delays has been improved with the addition

of a precise translation stage to the grating writing facility. The translation stage has a position accuracy of 1 mil ( $25.4\mu$ ). This would correspond to a time delay accuracy of 0.25 ps,  $(2 \times l \times n)/c$ . Other factors, such as the precise effective grating center, probably increase this error to 2-3 ps.

#### 4.0 Experimental Results

The experimental results produced during the period of performance of the True Time Delay program are presented here. These results include the measured reflectivity spectrums of the various types of fibers used, the measured RF response of the fiber gratings and the time delay measurements of multiple gratings. Also included here are general fiber grating characteristics that are relevant to the Fiber Bragg True Time Delay concept.

Early in the program an intense effort was undertaken to find suitable readily available fibers that gratings could be written in. Over the course of the program other fibers were added to the list and the table below summarizes the fibers that were used in this program and the results achieved with those fibers.

Fiber name	Index step %	molar % Ge	na	core size	highest R written	comments
Andrews Series E	2.4	23	.32	2x4 $\mu$	85%	polarization maintaining, birefringence $\delta n/n=1.5 \times 10^{-4}$
Spectran	0.33	3.5	.12	9 $\mu$	23%	
AT&T Accutether 220	1.1	11.58	.22	6.4 $\mu$	100%	single mode @ 1500nm
AT&T dispersion compensating fiber	1.7	17.9	.27	3.8 $\mu$	100%	single mode @ 1300&1500nm

Table 4-1. Fiber types used in the True Time Delay Program.

The % Germanium is noted in the table because the germanium concentration is a good indicator of the UV sensitivity or how well we can write gratings in the fiber. Note that we can write gratings in fibers that are single mode at 1300 nm and 1500 nm with the AT&T (Lucent) dispersion compensating fiber which we discovered just recently and that we can write gratings in polarization preserving fiber. The use of polarization preserving fiber opens the possibility of a polarization specific True Time Delay element

which would have the advantage of a lower insertion loss. The loss in the True Time Delay device is dominated by the optical circulator used which at present is polarization independent. Polarization dependent optical circulators can be made with significantly lower loss because fewer optical elements are required.

The first fiber type that was used was the Andrews Series E polarization preserving fiber. As noted in the table, this fiber has an elliptical core. The fiber is birefringent having a different index of refraction for each axis of the ellipse. The transmission spectrum of a grating written in this fiber is shown below in Figure 4-1. Because there are two different indices involved, there will be two separate effective Bragg gratings which are somewhat apparent from the two peaks shown in the figure. Recall the Bragg wavelength is given by  $\lambda_B = 2n\Lambda$  so that the wavelength separation of the two gratings is  $\Delta\lambda_B = 2(\Delta n)\Lambda = \lambda_B (\Delta n)/n$ . From Table 4-1  $\delta n/n = 1.5 \times 10^{-4}$  so  $\Delta\lambda_B = 0.2$  nm which is what is observed.

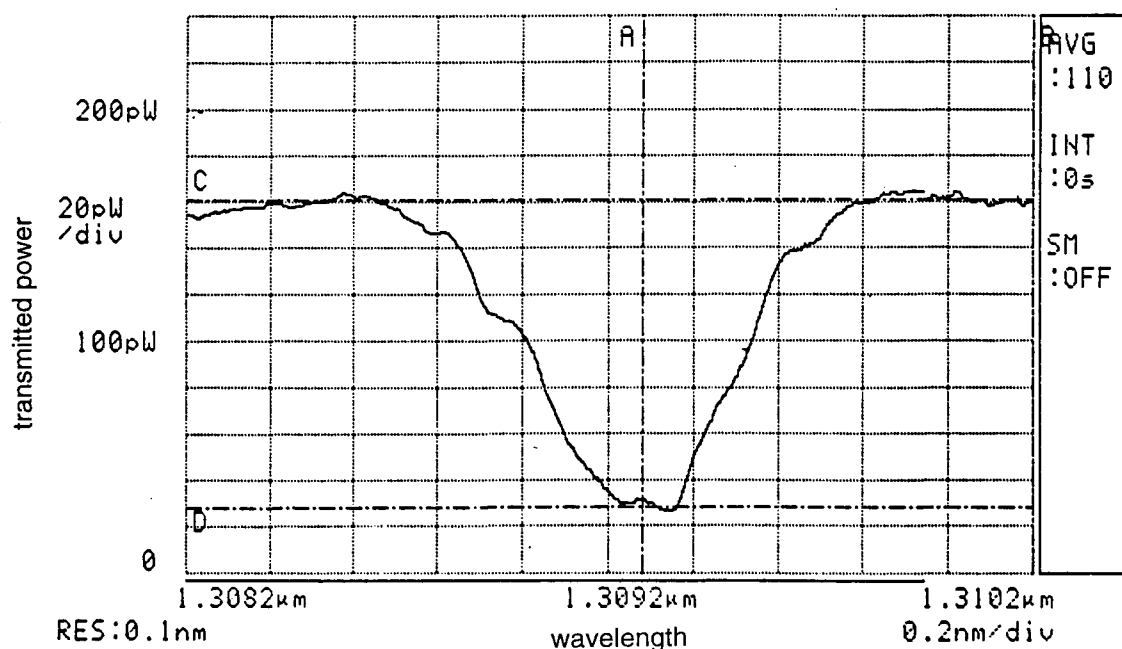


Figure 4-1. Bragg fiber grating transmission spectra of Andrews Series E polarization preserving fiber.  $R = 1 - \text{transmission} = 1 - (26 \text{ pW}) / (160 \text{ pW}) = 84\%$

Other spectra taken with the other fiber in the table are shown in Figure 4-2 a,b, and c.

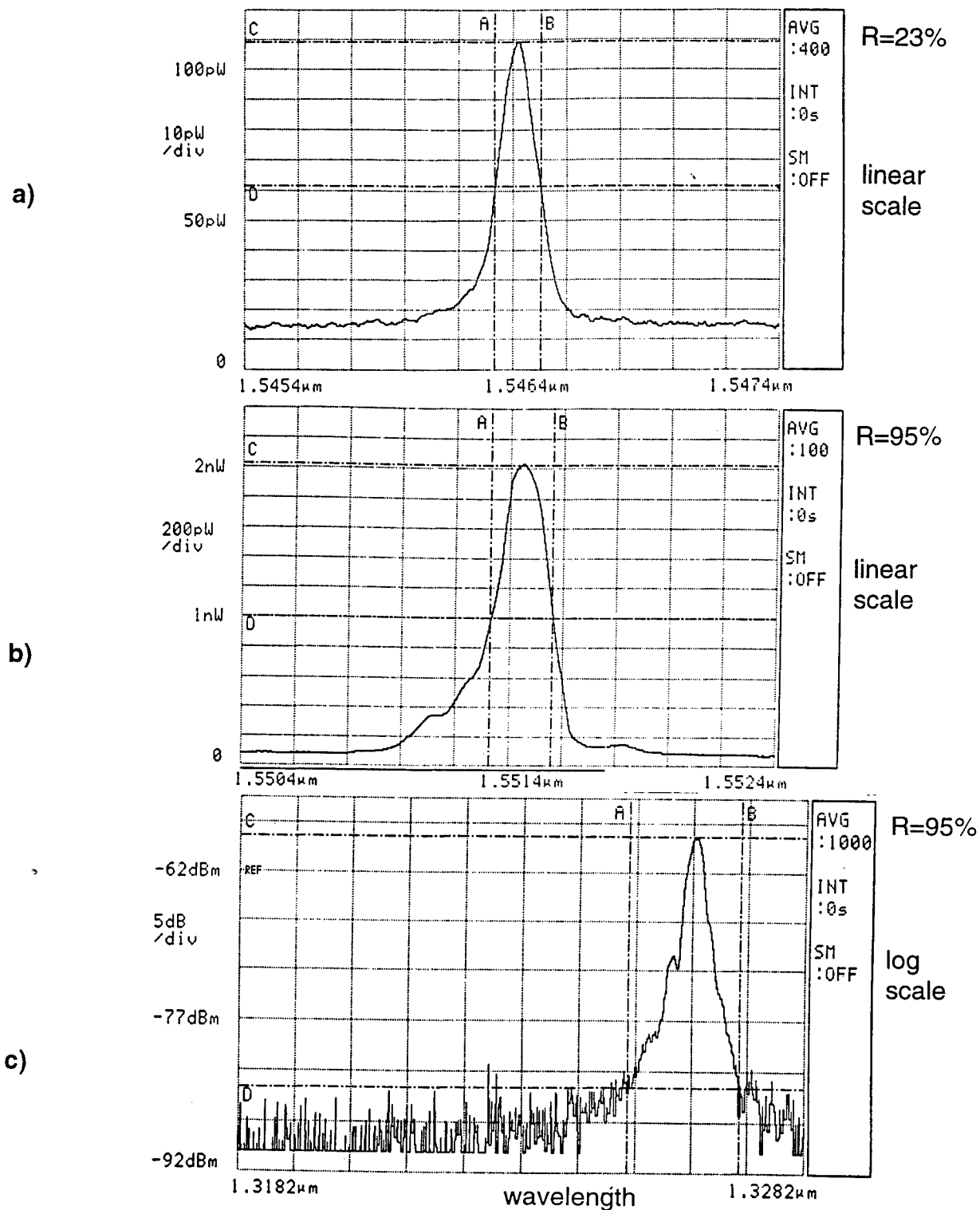


Figure 4-2. Optical reflectivity spectrum of a) Spectran b) AT&T Accutether 220 and c) AT&T dispersion compensating fiber

The writing speed that was observed for the various types of fibers was similar. When the focus of the cylindrical lens was tight, 3-5 microns, the writing time was very short. 80% reflectivity could be achieved in 90 seconds. However, when the focus was tight the alignment was more critical, The core size as noted in Table 4-1 was around the size of the focus or even larger in the case of the Accutether 220. A looser focus is preferred so that the writing beam was larger than the core diameter. In this way the core was illuminated more uniformly. In Figure 4-3 is shown the writing times for two types of fibers written with the looser focus.

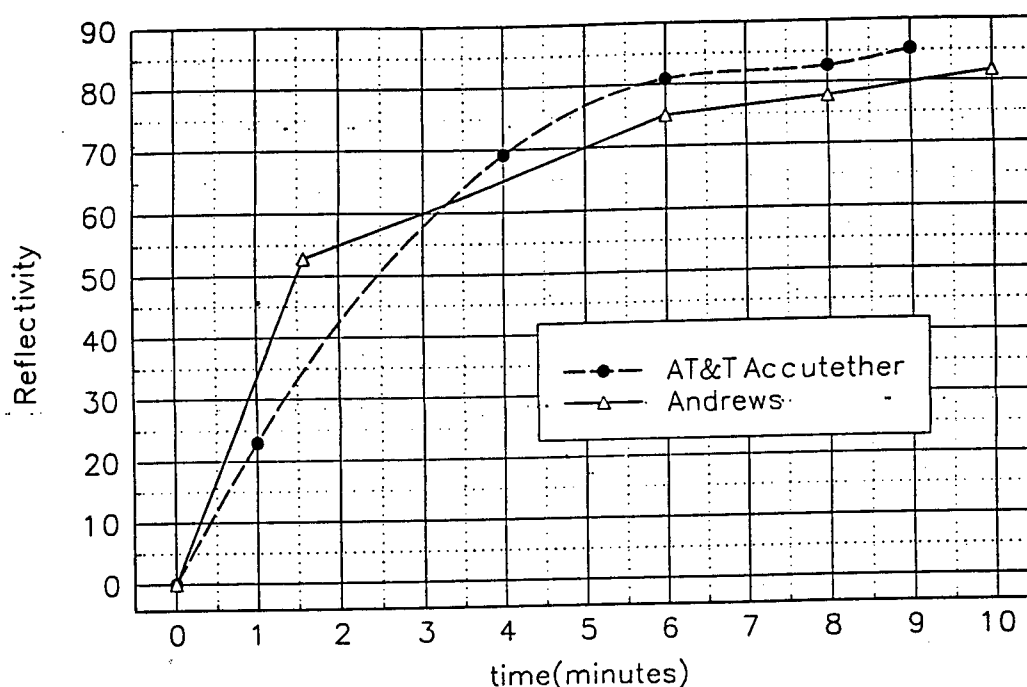


Figure 4-3. Reflectivity vs. Time for Andrews Series E fiber and AT&T Accutether 220 single mode fiber for loose focus writing.

As noted in section 3.0, Grating Writing Facility, the fiber was under tension while the Bragg grating was being written. This was done to keep the fiber steady and to avoid droop in the fiber over it's one inch suspension. The shift in wavelength of the Bragg reflectivity center is plotted as a function of fiber tension and is shown in Figure 4-4.

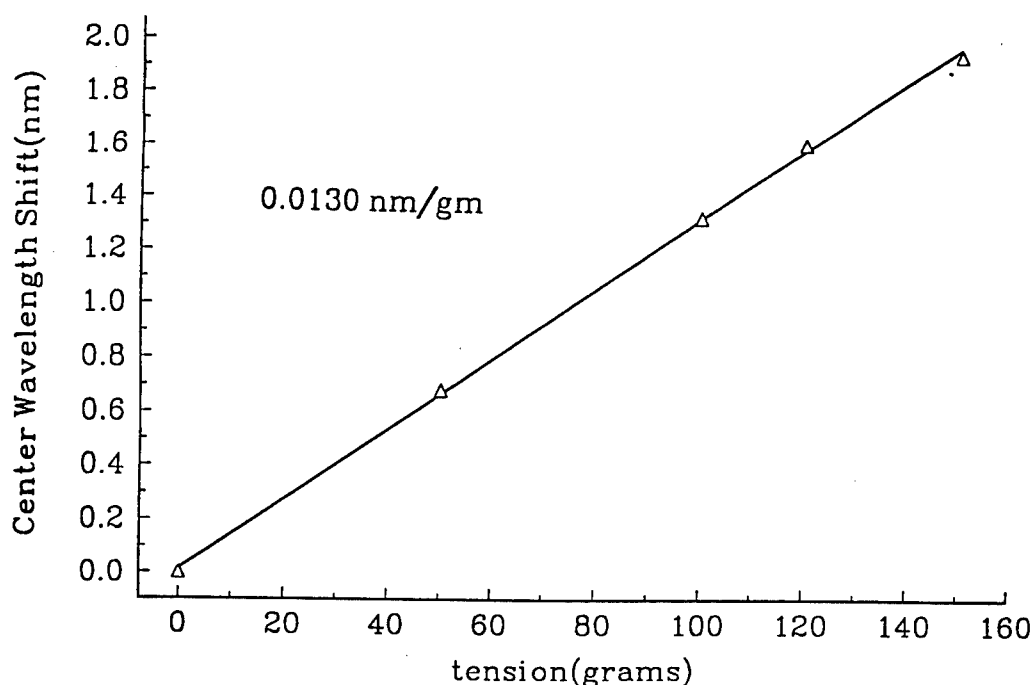


Figure 4-4. Grating center wavelength shift vs. tension. The slope is 0.013 nm/gm for the Accutether 220 type fiber.

The Bragg grating center wavelength also shifts with temperature due to the change in the index of refraction as well as the change in length. The relationship between fiber temperature and wavelength shift is given below. For quartz fiber,

$$\frac{\Delta\lambda}{\Delta T} = \left[ \frac{1}{n} \cdot \left( \frac{dn}{dT} \right) + \frac{1}{L} \cdot \left( \frac{dL}{dT} \right) \right] \cdot \lambda$$

the constant in the brackets is  $8.8 \times 10^{-6}$ . This temperature effect is noted as the Bragg gratings are being written. The focused UV writing beam heats the fiber while it's being written. It was noted that the wavelength shifts 0.08 nm which implies a temperature rise of 5.86°C.



## SIDELobe SUPPRESSION

Another key parameter for the TTD application is the channel isolation for each grating. Ideally, only one grating should have any reflection for a given wavelength. In practice this isolation is measurable and as the wavelength separation of any two gratings decreases, the isolation decreases. The type of grating writing profiles that we have been using to date is a half gaussian profile. For improved isolation one wants a smoother profile, more like a full gaussian. To achieve this we have rotated the fiber relative to the tight line focused UV writing beam. At the sharp edge of the half gaussian line focus profile, the fiber is positioned to just miss the focus. At the smooth tapered end of the half gaussian, the fiber is fully in the line focus. The resulting grating writing profile has a shape as shown by the dashed line below in Figure 4-5. The solid line is the previously used hard half gaussian profile.

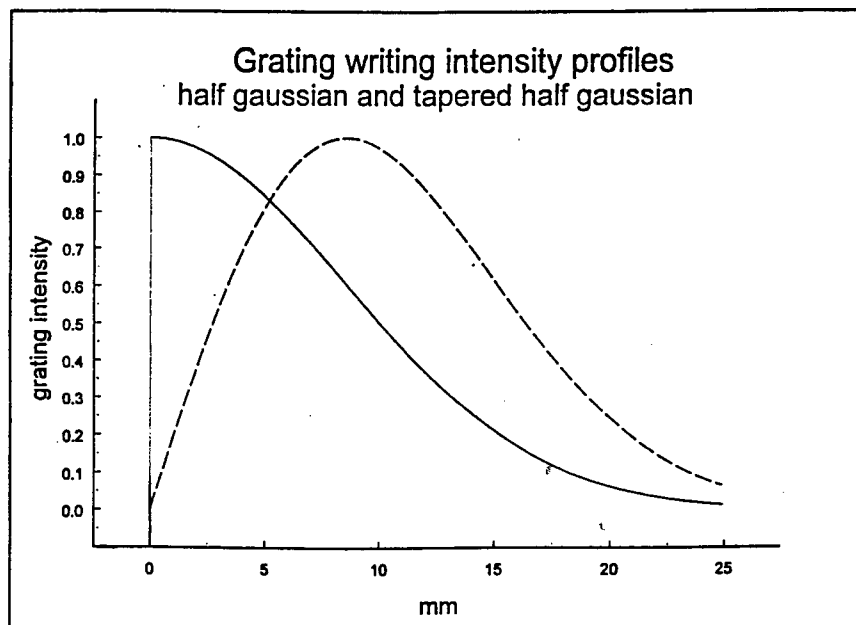


Figure 4-5. Half Gaussian and new "soft" modeled grating writing intensity profiles.

The improvement in the reflectivity profile is shown in Figure 4-6 b). In Figure 4-7 the channel isolation is plotted vs. channel width for half gaussian and “soft” intensity writing profiles.

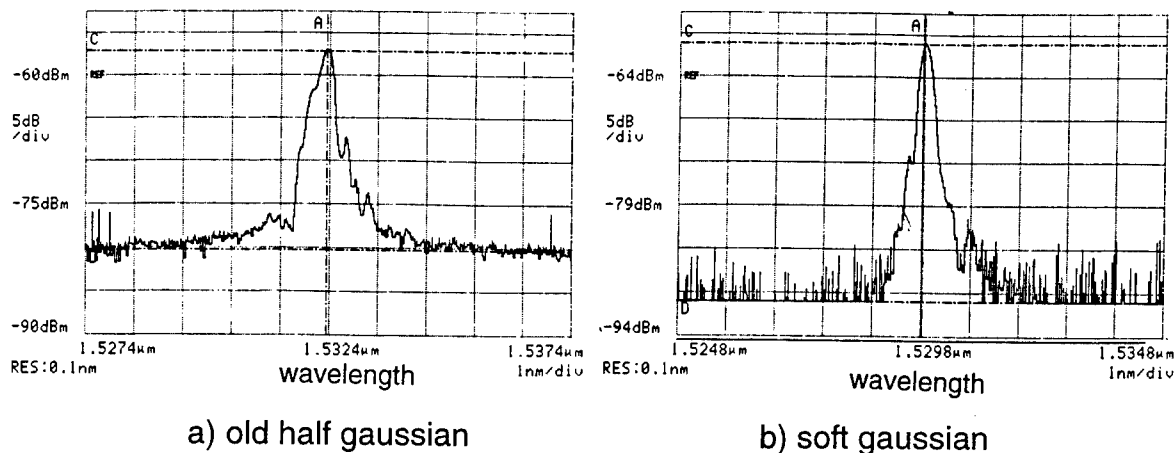


Figure 4-6. Reflectivity profile for the old half gaussian a) and new “soft” gratings b).

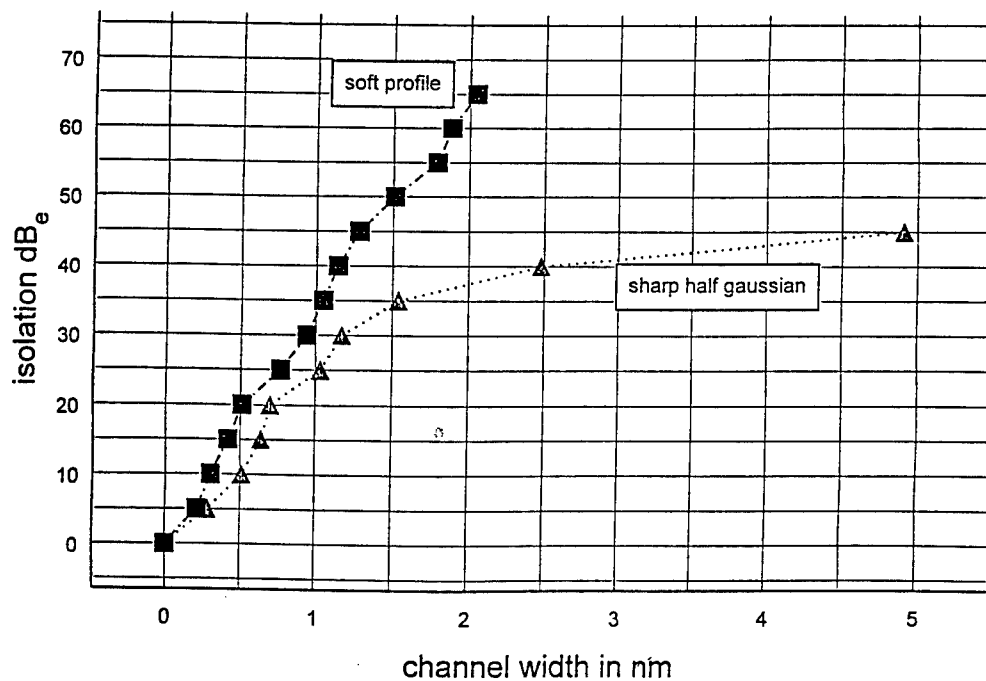


Figure 4-7. Channel isolation vs. channel width for half gaussian and “soft” gratings.

The improvement means that for a given tuning range of the optical carrier laser source and a given desired channel isolation, one can have many more gratings, thus more bits of time delay accuracy.

## RF CHARACTERIZATION

As indicated in the modeling section of this report, the RF phase error is very small. As long as the optical center frequency stays within the strong optical response portion of the grating (full width half maximum), then the variation in the RF response will be small. For large desired RF bandwidth the grating can be made to be as broad as is needed. The computer model predicts that within the useful portion of the grating, the RF phase is very linear and varies only a few degrees. We have verified this in the lab with the setup diagrammed in Figure 4-8. To determine the RF characteristics a 1550 nm optical carrier was amplitude modulated from 100 MHz to 3 GHz. The modulated signal reflected from a fiber optic grating was measured with a network analyzer to determine both the RF phase and amplitude response of the grating as a function of the RF frequency. The RF amplitude follows the shape of the optical response as does the phase. The phase variation was very small, less than a few degrees, over the frequency span observed.

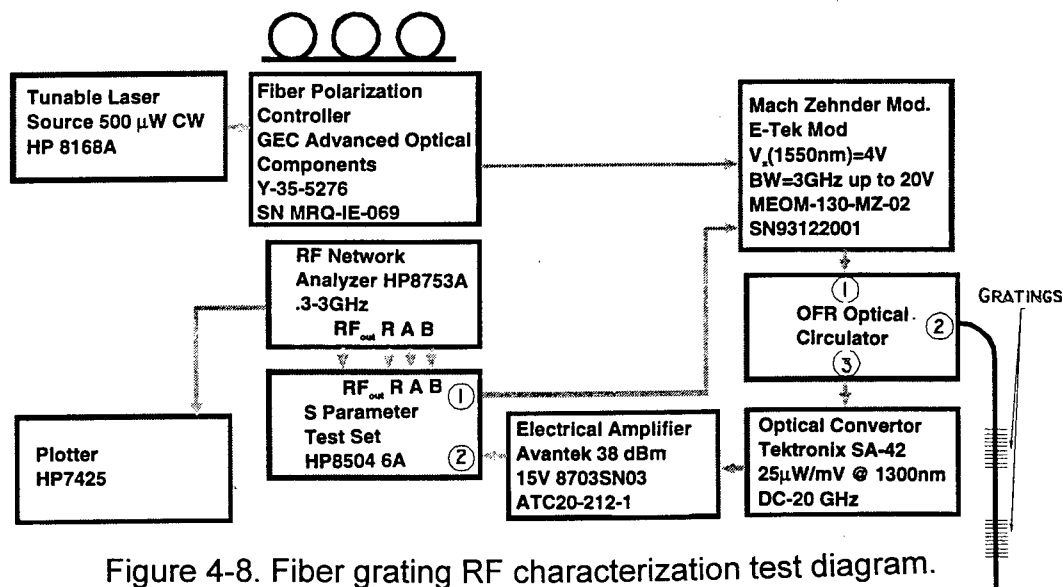


Figure 4-8. Fiber grating RF characterization test diagram.

The measured RF phase from 0.3-3 GHz is shown in Figure 4-9. To the accuracy of the measurement the phase variation was much smaller than the phase contribution of the measurement apparatus which was canceled in this measurement.

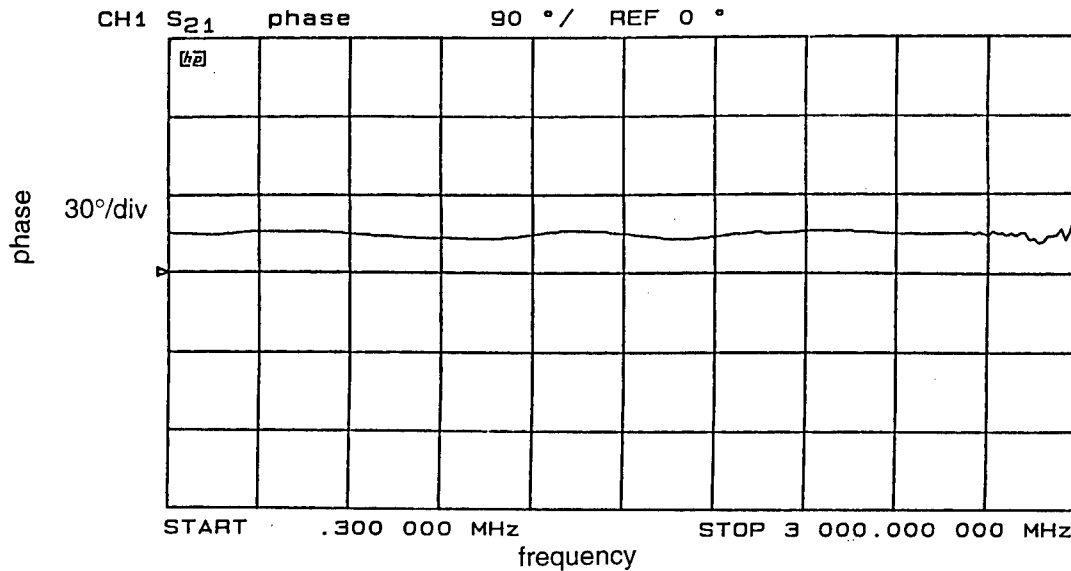


Figure 4-9. RF phase measured from 0.30 to 3.0 GHz. The laser was tuned to the center frequency of the Bragg grating,

This is not an unexpected result and as long as the optical carrier frequency is within the full width half maximum of the Bragg grating then the phase error will be very small. Thus small drifts in the optical carrier frequency will have minimal detrimental impact to the overall system performance.

## TIME DELAY ACCURACY

One of the key parameters to control in the TTD application is the time delay itself. The precision that we can make time delays has been improved with the addition of a precise translation stage to the grating writing facility. The translation stage has a position accuracy of 1 mil (25.4 $\mu$ m). This would correspond to a time delay accuracy of 0.25 ps. We have written 4 gratings at different wavelengths and have measured the time delay. The grating spacings were equal and controlled to the accuracy of the

translation stage, 25.4 $\mu$ m. The time delay of pulses reflected from each of the four gratings were measured using the equipment shown in Figure 4-10 below. The measured time delays from the gratings is shown in Figure 4-11. To the accuracy at which we could measure them, 20 ps, the time delays were exactly equal spaced. The accuracy was limited by the frequency response of the 3 GHz Mach Zehnder modulator that was used.

An accuracy of 1 ps should meet requirements with margin. It was also determined that we could write gratings at two different wavelengths at exactly the same position as would be required for identical time delays. It was observed that the reflectivity of the first grating decreases from 90% to 60% as the second grating is written.

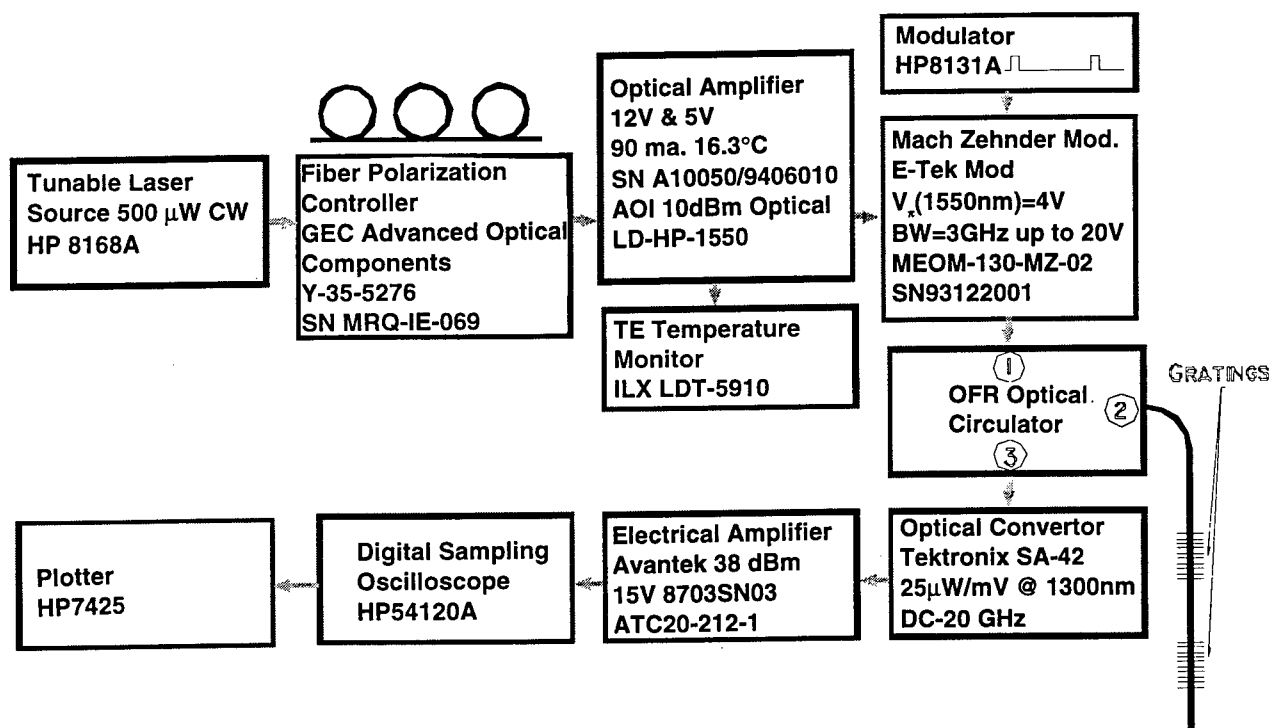


Figure 4-10. Time delay measurement apparatus.

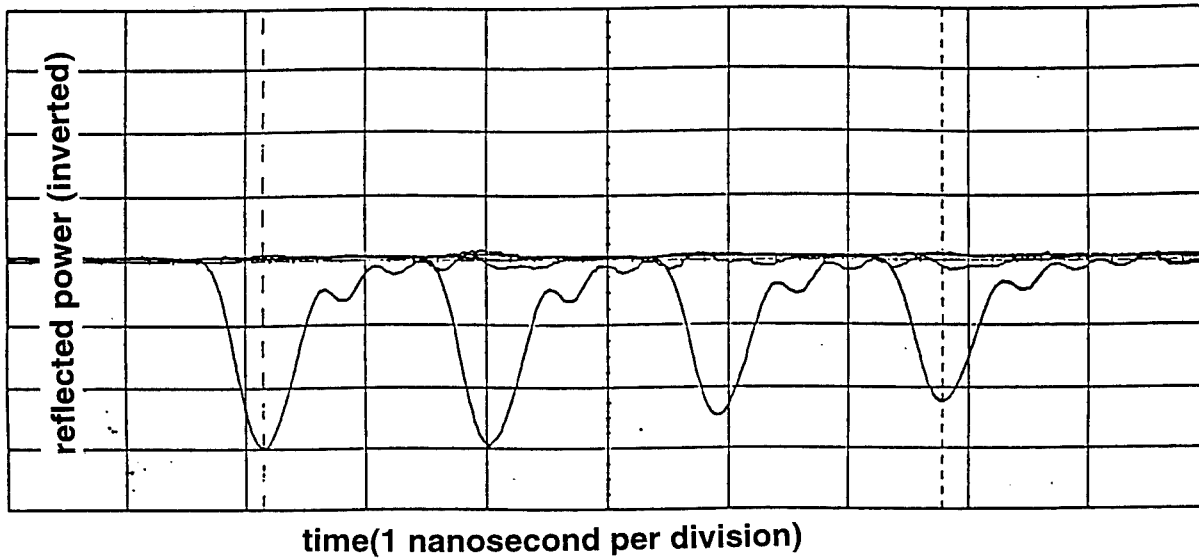


Figure 4-11. Measured time delay pulses from 4 equally spaced gratings.

## 5.0 True Time Delay Deliverable

The True Time Delay deliverable is a 4-bit device. The 16 gratings, each written at different wavelengths, are on a single fiber and are equally spaced. The spacing is actually arbitrary for any one time delay element. It is the time delay between sub-array elements that is important. The time delay between elements should have errors corresponding to less than a fraction of an RF wavelength or several picoseconds at RF frequencies of interest. The method that we have developed for setting the spacing, described earlier, meets this requirement. The spacing between each grating is 10 cm (500 ps) and has an accuracy of 1-2 picoseconds.

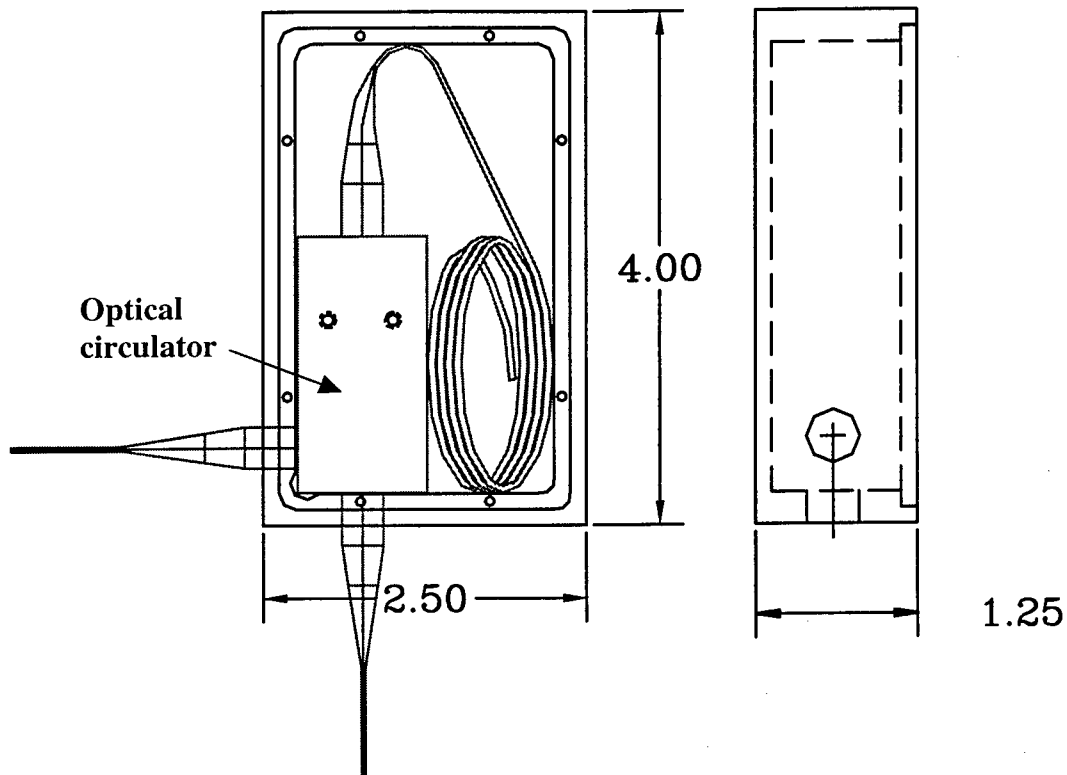


Figure 5-1. True Time Delay deliverable. Dimensions are in inches and there is a APC connector union at the fiber (not shown) to facilitate the exchange of the grating fiber.

The TTD deliverable is very small as shown in Figure 5-1 above where the dimensions indicated are in inches. The small box, inside the somewhat larger box, is the optical circulator. The 16 gratings are in the coiled fiber next to the optical circulator and the fiber is terminated with index matching epoxy to minimize end reflections. The coiling of the fiber gratings does not deteriorate their performance. We have coiled fiber gratings with radius of curvatures as small as 1/2 inch without any change noted in the optical reflectivity spectrum. There is a very small loss when fiber is coiled due to enhance clad mode coupling but for such short lengths of fiber the loss is still very small compared to the loss incurred due to the optical circulator,  $2 \text{ dB}_{\text{optical}}$ , or even the when compared to the reflectivity loss when  $R=80\text{-}85\%$ . With a more current optical circulator, the overall package can be smaller than the one shown in Figure 5-1. In Figure 5-2 is shown the current package next to the package size that could be obtained with a JDS Fitel optical circulator which is now available.

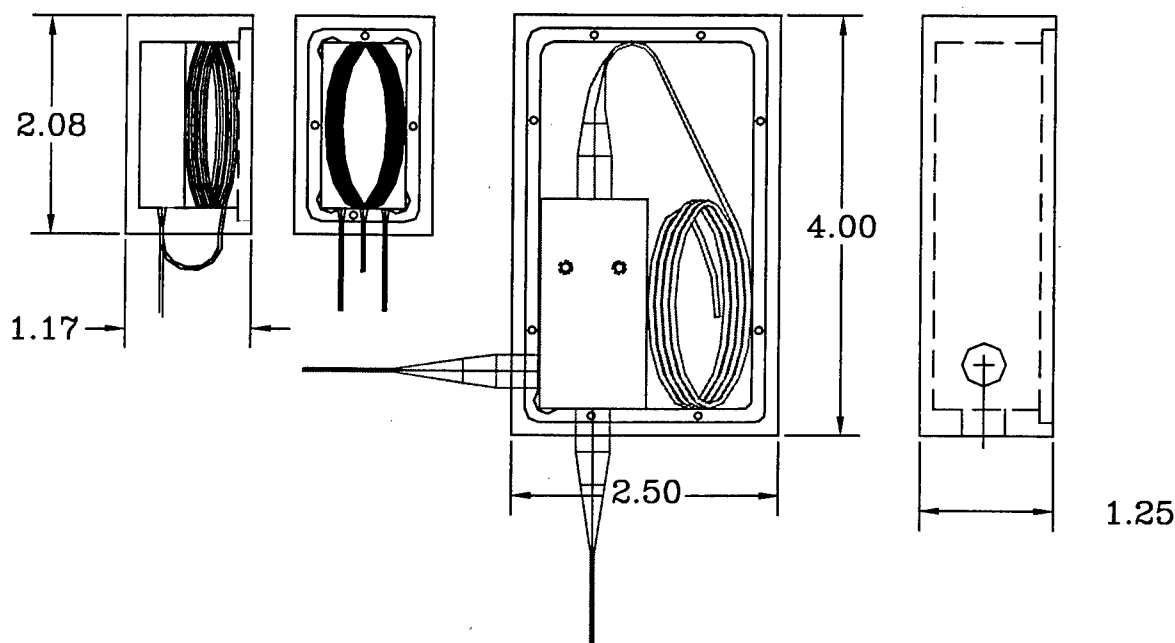


Figure 5-2. True time delay package size with Optics for Research circulator (right) and the new JDS Fitel circulator (left).



Two 4-bit time delay fibers were written on two types of fibers. The first attempt proved to be inappropriate because the fiber used, AT&T Accutether 220, is not single mode at 1300 nm but is single mode at 1500 nm. A transmission spectrum of this fiber is shown below in Figure 5-3 and in Figure 5-4 is shown the reflectivity for each of the gratings. The variation in reflectivity is due to the multimode nature of the gratings.

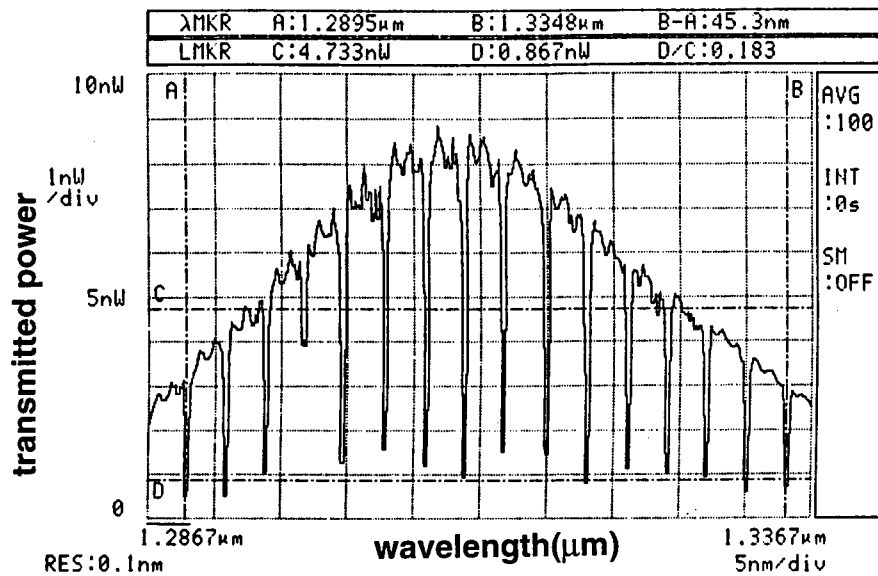


Figure 5-3. Transmission spectrum of 16 grating fiber. Gratings were written in AT&T Accutether 220 fiber.

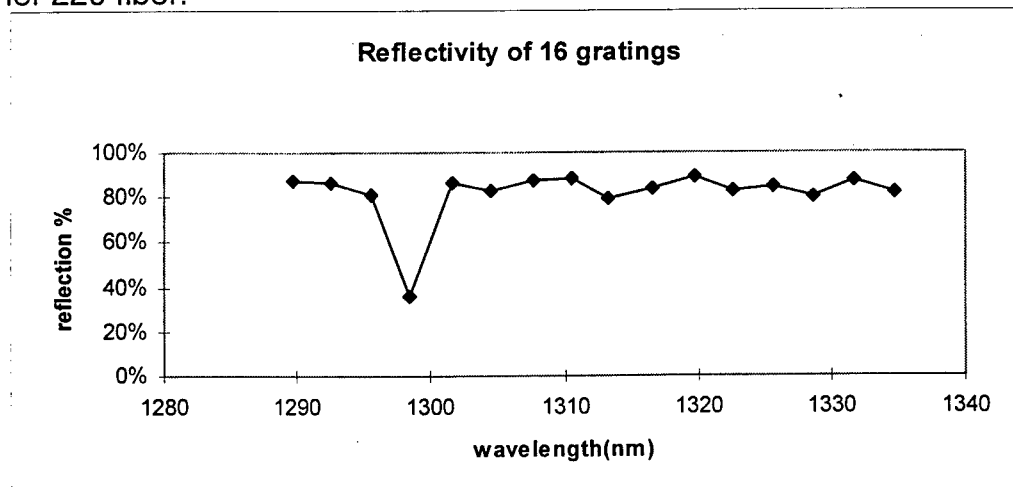


Figure 5-4. Measured reflectivity for each grating.

	mean	standard deviation
wavelength separation	3 nm	0.12 nm
reflectivity	82.0%	1.85%
channel isolation	40 dBe	not measured
channel physical separation	10 cm	not measured

Table 5-1. Measured parameters of the first 16 grating

As noted above, the fiber that we used to write the gratings shown in Figure 5-3, is AT&T Accutether 220 and is single mode for 1.5  $\mu\text{m}$  light. At 1.3  $\mu\text{m}$  more than one core mode can propagate with low loss if the light is not launched optimally. The higher order modes have a higher group velocity (lower effective index of refraction) and reflect off the gratings at a lower wavelength than the fundamental mode. As a consequence, the gratings written in this fiber at 1300 nm will reflect at two or more wavelengths as shown in Figure 5-5. The core diameter of the AT&T Accutether 220 is 6.4  $\mu\text{m}$  and calculations indicate that the fundamental as well as 2 higher order modes can propagate with low loss. If the light is coupled optimally for the fundamental, then only one reflection is observed. However, as the coupling is varied, the ratio of energy into the available modes can vary considerably and is difficult to control. Fortunately, AT&T makes another type of fiber that has a core diameter of 2.8  $\mu\text{m}$  and is single mode at 1.3  $\mu\text{m}$  and 1.5  $\mu\text{m}$ . It also has a high germanium doping and thus good UV sensitivity. Excellent gratings have been written in this fiber as shown in Figure 5-6. The secondary gratings are completely gone.

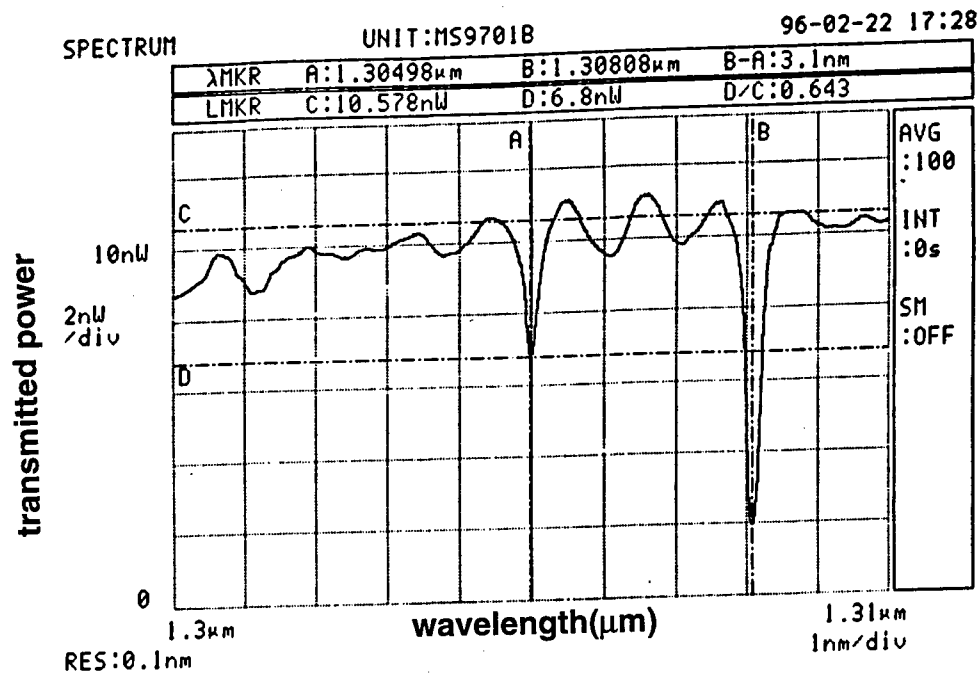


Figure 5-5. Reflectivity spectrum of grating written in Accutether 220 showing main reflectivity peak at 1308 nm and secondary reflectivity peak at 1305 nm.

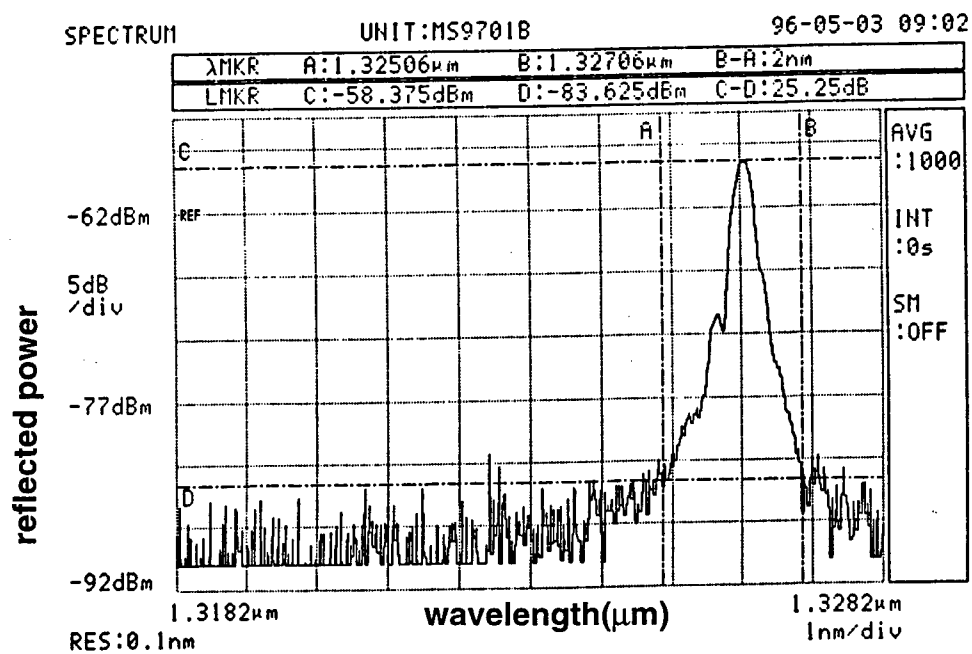


Figure 5-6. Reflectivity spectrum of grating written in AT&T's Dispersion compensating fiber at 1326 nm.

A second 16 grating fiber was written using the AT&T's Dispersion Compensating (DC) fiber that is single mode at 1300 nm. This fiber was brought to our attention by David Peckman at AT&T who also gave us a generous sample(2500 m). We have readily available fibers that we can write 100% reflectivity single mode gratings without the need for hydrogenation. Because we don't need to load fiber with hydrogen to make them UV sensitive, these gratings are more robust, will have a longer lifetime, and be less radiation sensitive.

Shown in Figure 5-7 is a transmission spectrum of the 16 grating DC fiber and in Figure 5-8 is shown the measured reflectivity for each grating. The overall shape of the transmission curve is dominated by the output spectrum of the LED source. The mean reflectivity was chosen to be around 87%. The choice of reflectivity is a compromise between high reflectivity and channel separation. As the reflectivity increases, the grating width in wavelength also increases and so the channel isolation decreases. The 16 gratings were written over a period of a few days. To precisely locate the wavelength position of each grating, a test grating was written in a separate fiber before each grating in the deliverable fiber was written. The figures of merit for this 16 grating fiber are shown in Table 5-2 and the wavelength positions are shown in Table 5-3.

The time delayed pulses were recorded using the equipment indicated in Figure 4-10 and the results of the measurement are shown in Figure 5-9. Figure 5-9 is a composite created by overlaying the 16 reflected pulses as the wavelength was tuned to the 16 different Bragg wavelengths of the 16 gratings in the True Time Delay deliverable fiber. The accuracy of the 16 individual time delays is indicated in Figure 5-10 where the time delay is plotted vs. the grating number. The attempt was to make the time delay between each successive grating equal and Figure 5-10 demonstrates, to the accuracy of the measurement, how well we succeeded. In the future we will determine, with more accuracy, how well that we can create a specific time delay.

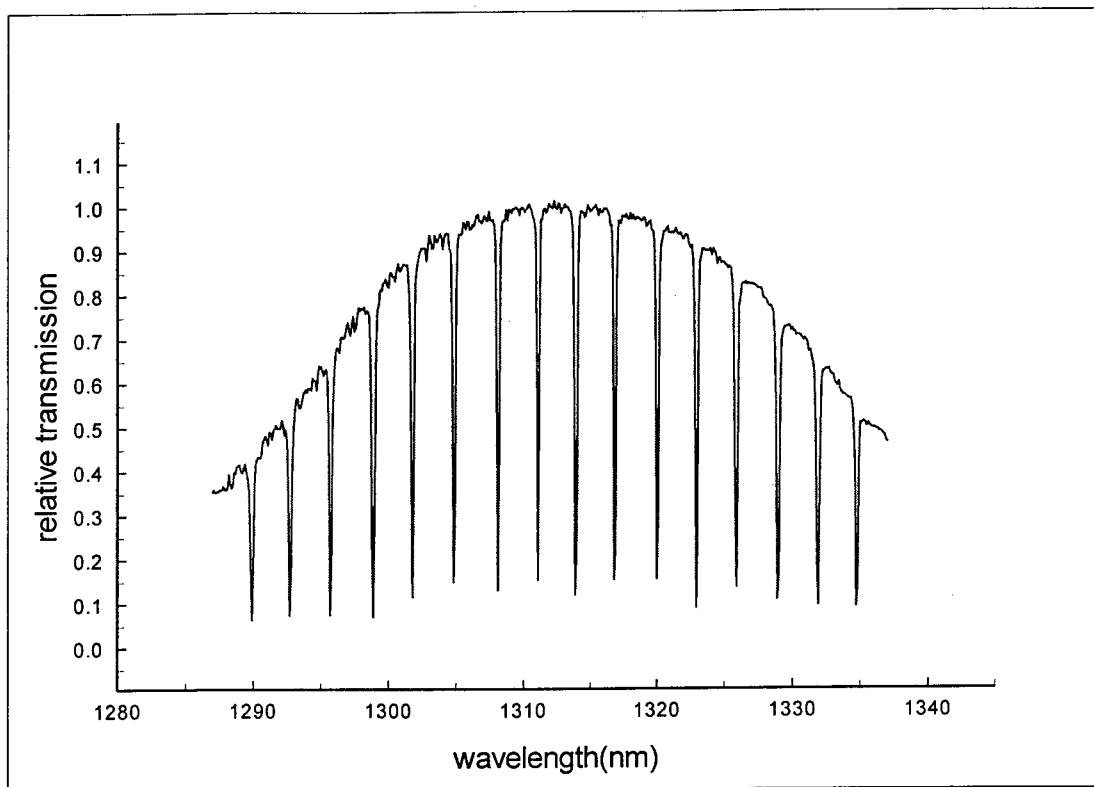


Figure 5-7. Transmission spectra of 16 grating fiber.

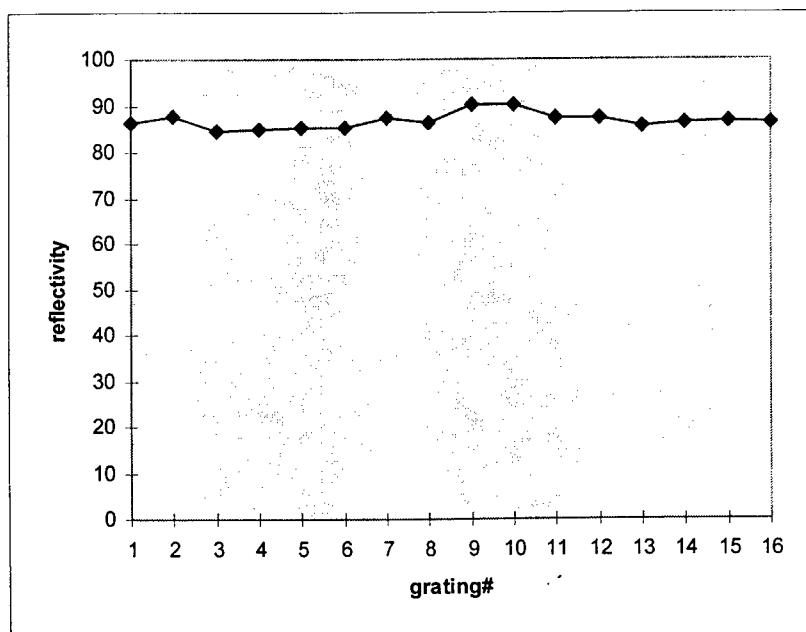


Figure 5-8. Measured reflectivity for each grating.

	mean	standard deviation
wavelength separation	3 nm	0.0437 nm
reflectivity	86.72%	1.65%
channel isolation	60 dBe	not measured
channel physical separation	10 cm	not measured

Table 5-2. 16 grating measured parameters

grating number	center wavelength in nm	Peak Reflectivity (%)
1	1290.42	86.4
2	1293.33	87.8
3	1296.40	84.5
4	1299.44	84.8
5	1302.31	85.2
6	1305.38	85.3
7	1308.46	87.4
8	1311.38	86.2
9	1314.35	90.2
10	1317.37	90.1
11	1320.40	87.2
12	1323.40	87.3
13	1326.44	85.5
14	1329.44	86.4
15	1332.34	86.8
16	1335.37	86.4

Table 5-3. Center wavelength positions and peak reflectivity for the 16 gratings in the True Time Delay deliverable.

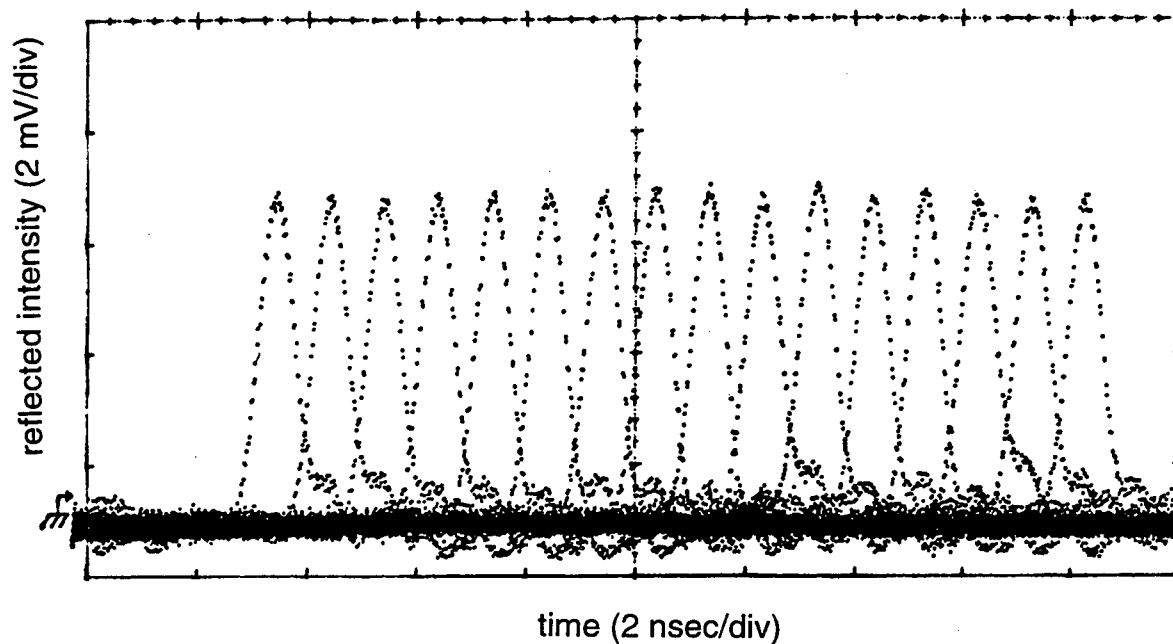


Figure 5-9. Time delayed pulses from the 16 grating True Time Delay deliverable

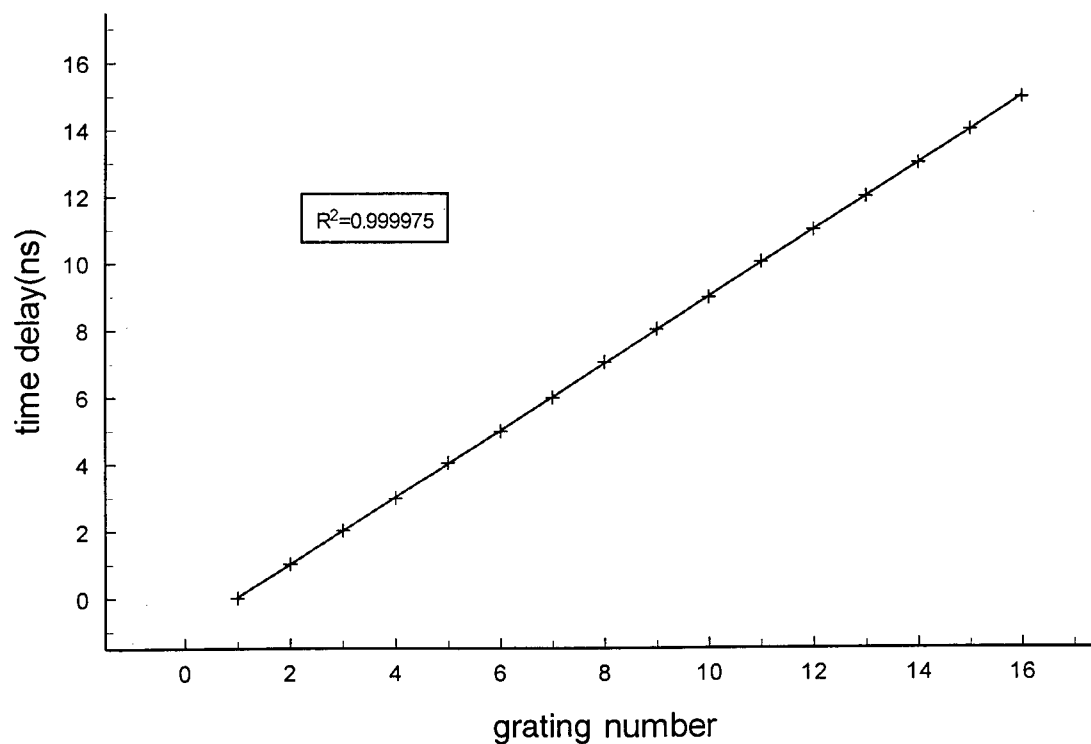


Figure 5-10. Time delay vs. Grating number and linear fit to the data.

## 6.0 Planar Silica Waveguides and Hydrogen Loading

To extend the capabilities of the True Time Delay technology, the writing of Bragg gratings in planar silica waveguide material was undertaken. The material was purchased under contract from the PIRI Corporation<sup>4</sup>. Silica-based optical integrated circuits are fabricated on Si substrates, or Quartz substrates in our case, by the combination of flame hydrolysis deposition and conventional photolithography techniques followed by reactive ion etching. The fabrication technique results in the following advantageous features: low waveguide propagation loss of 0.1 dB/cm or less, extremely low fiber-waveguide coupling loss due to almost complete field matching, and high precision waveguide length setting by photolithography techniques.

Six pieces were purchased from PIRI each of which had 8 straight waveguide channels, 8  $\mu\text{m}$  by 8  $\mu\text{m}$  in cross section. The physical structure of the devices is shown in Figure 6-1. The eight straight waveguide channels have single mode fiber

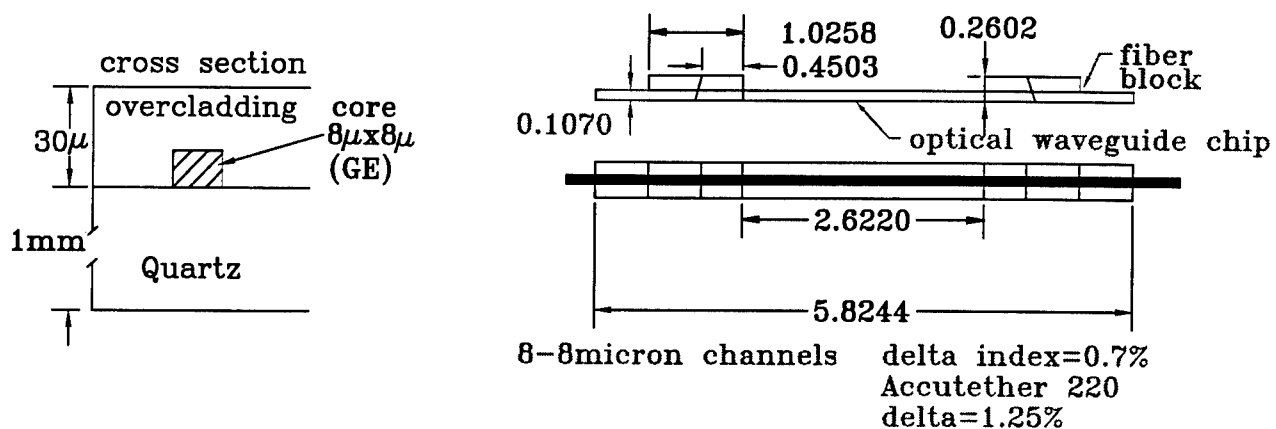


Figure 6-1. Silica planar waveguide structure purchased from PIRI.

ribbon attached to each end of the device. The dimensions are shown in cm. The germanium doped 8x8 $\mu\text{m}$  core has an index step of 0.7% delta in the index of

<sup>4</sup> PIRI, Inc., Photonic Integration Research, Inc., 2727 Scioto Parkway, Columbus, OH 43221-4658, (614) 876-5655.



refraction,  $n_{\text{core}} = 1.46106$  and  $n_{\text{clad}} = 1.4509$  @  $1.3 \mu\text{m}$ . The fiber that we are currently using, AT&T Accutether 220, has a delta of 1.25% and we can write gratings approaching 100% reflectivity and so it was anticipated that we should have been able to write good gratings in this waveguide material. We could not. After a small modification to our grating writing facility, we attempted to write gratings in this material and got absolutely no response. On the surface, the properties of the waveguide material seemed to indicate that the material should have good UV sensitivity. The molar concentration of germanium in the material is 64% of what it is in the AT&T Accutether 220, usually a prime indicator of good UV sensitivity. However, the UV sensitivity comes from the defect center density which not only depends on the germanium concentration but also the method of production. Something in the method of production of the planar silica waveguide material does not encourage the growth of the UV sensitive defect centers. Evidently the manufacturing process for the single mode fibers that we've written gratings in, creates the defect centers that absorb UV at 244 nm and that process that is used for this silica planar waveguide material does not create those same defect centers or creates a different type of defect center. A high germanium doping is not a sufficient requirement for UV sensitivity.

To be able to write gratings in this material it must be loaded with hydrogen. Others have reported that hydrogen loading has proven successful in increasing the UV sensitivity of fibers and planar silica waveguide material. To this end, a hydrogen loading facility was designed and built on TRW funds. The cell that was made is shown in Figure 6-2. The cell and its contents are operated at 1500 PSI for at least one week. Loading time could be reduced if the cell temperature is higher but this was not attempted. The cell is 2 feet long and has an inner diameter of 1 inch. To put long fibers into the cell a bend radius of 0.5" or 1.3 cm has to be tolerated by the fibers. The fibers attached to the planar silica waveguide material and all of the fibers that we use, can tolerate that bend radius with some margin. One piece of the silica planar waveguide material and several meters of AT&T (Lucent) Dispersion compensation

fiber were placed in the cell at 1500 PSI for a period of 2 weeks. This exposure made the samples very UV sensitive and strong gratings were written in both planar silica

HIGH PRESSURE TEST CELL DWG# HYTESTCELL

USE ALL 316 STAINLESS STEEL

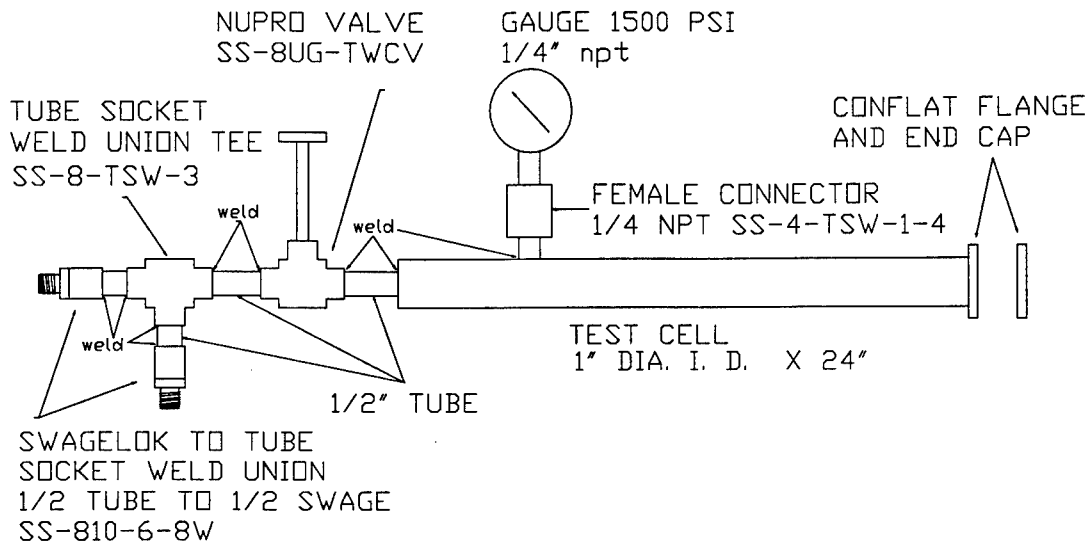


Figure 6-2. Hydrogen loading cell.

waveguide material and the single mode Dispersion Compensating Fiber. Two gratings were written in a single channel of the planar silica waveguide material. Figure 6-3 shows the transmission spectrum of that channel. The grating on the left was written over a 20 minute period and has a width of 5 nm. Note that the width of the gratings written in previously written gratings is only 0.15-0.20 nm. A second channel was exposed and the growth of the grating was recorded. The laser power was turned down to 20 mW (compared to >100 mW) for these exposures so that we could watch the early growth of the gratings. In Figure 6-4 is shown the transmission spectrum after 4 minutes of exposure. Note that two transmission dips are evident. This is due to the multimode nature of the waveguide at this wavelength. The channels are too large to be

single mode at 1.3  $\mu\text{m}$ . The width of the peaks,  $\sim 0.4 \text{ nm}$ , is already broader than the single mode widths that we're used to seeing. In Figure 6-5 is shown the transmission spectrum after 8 minutes of exposure when  $R=97.6\%$ . Note the additional structure.

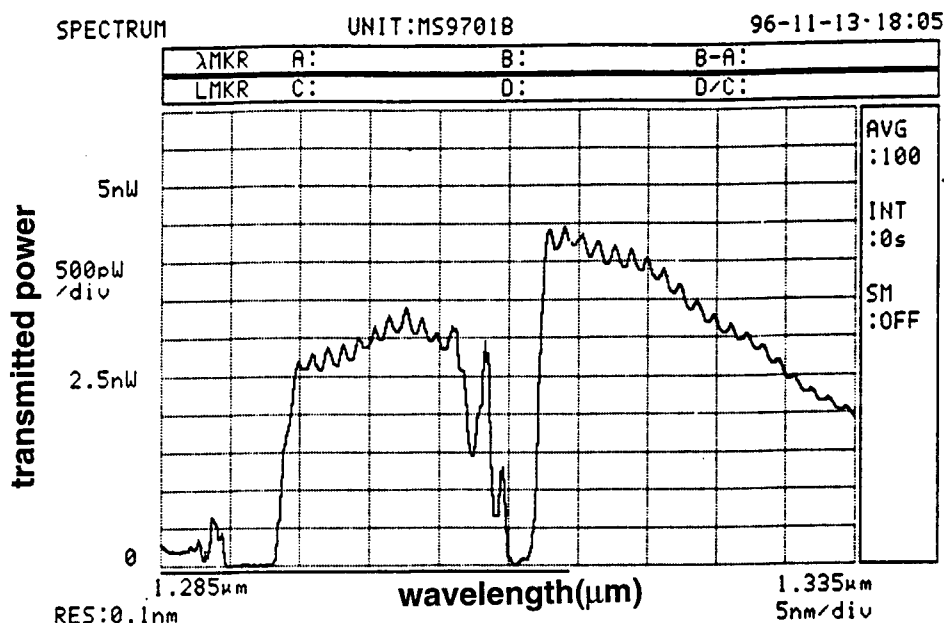


Figure 6-3. Transmission spectrum of the hydrogen loaded planar silica waveguide material after 2 Bragg gratings were written in one of the channels.

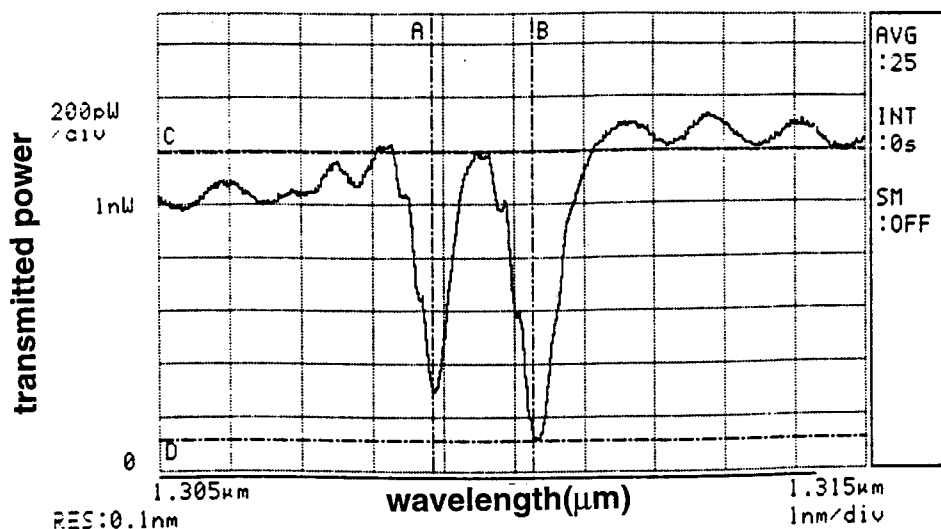


Figure 6-4. Transmission spectrum of a single channel after 4 minute of exposure to UV.

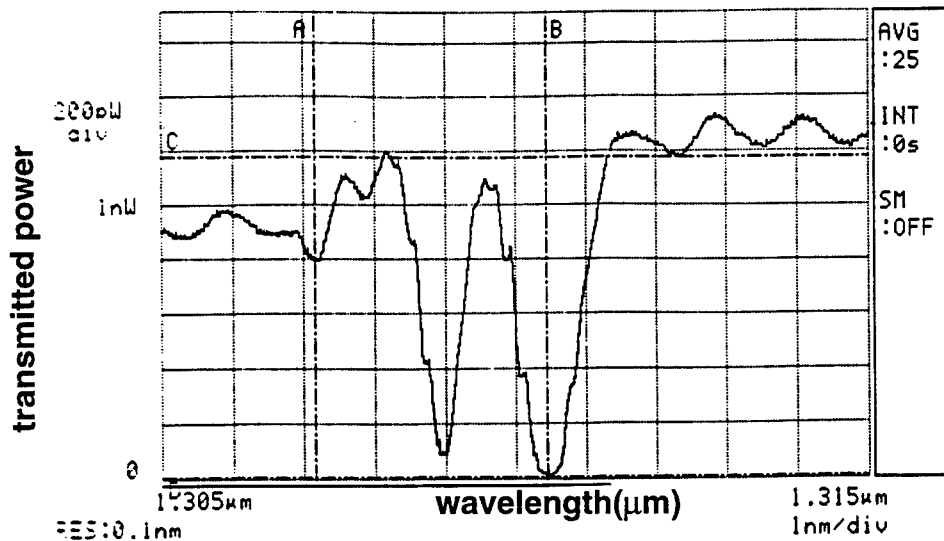


Figure 6-5. Transmission spectrum of a single channel after 8 minutes of exposure.

Continued exposure broadens the peaks until they merge into each other and resemble the peaks shown in Figure 6-3.

To complete the hydrogen loading study, we exposed a piece of hydrogen loaded, AT&T Dispersion Compensating Fiber to a 11 mW UV beam. In Figure 6-6 is shown a transmission spectra of this fiber after 10 seconds of exposure. The width of the spectrum is still quite narrow being only 0.25 nm. At a full minute the reflectivity is 100% and the width is 0.6 nm and in Figure 6-7 is shown the transmission spectrum after 11 minutes of exposure when the width has grown to 0.7 nm. As the writing process continues the spectrum broadens and the center wavelength shifts. The shift is due to a change in the mean index of refraction. From the initial low reflectivity center wavelength to the final center, 11 minutes later the total shift was 0.5 nm. This can be translated to a fractional change in the mean index of refraction:

$$\Delta\lambda/\lambda = \Delta n/n = (0.5 \text{ nm})/(1300 \text{ nm}) = 3.85 \times 10^{-4}.$$

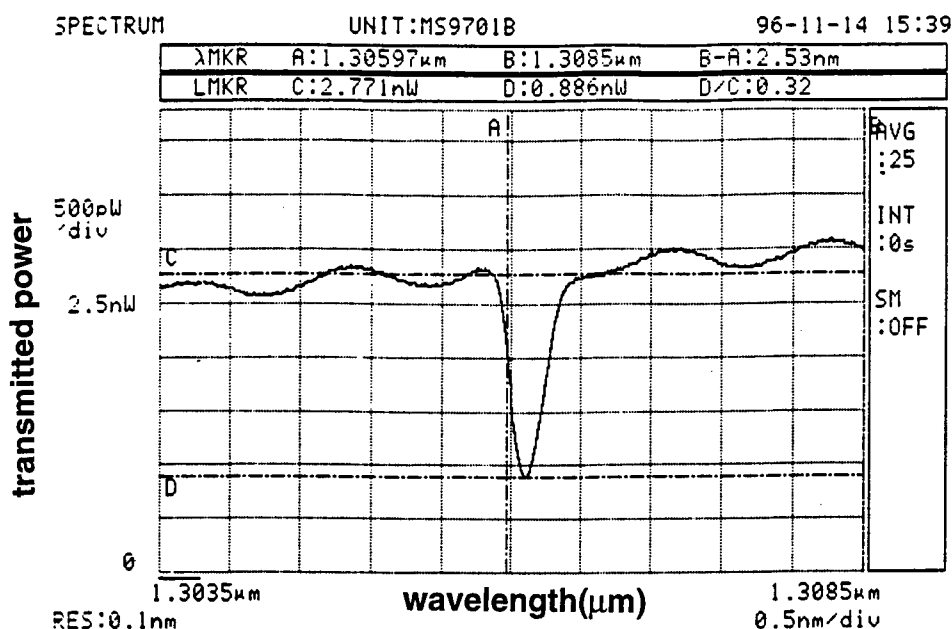


Figure 6-6. Transmission spectrum of Hydrogen loaded AT&T Dispersion Compensation Fiber after 10 seconds of exposure to a 11 mW 244 nm beam.

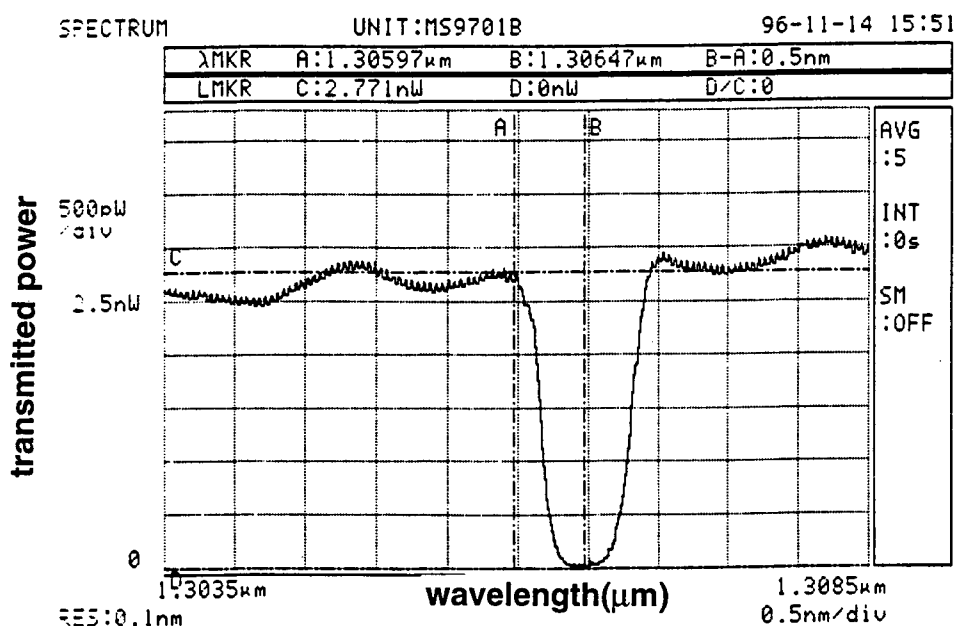


Figure 6-7. Transmission spectrum of Hydrogen loaded AT&T Dispersion Compensation Fiber after 11 minutes of exposure to a 11 mW 244 nm beam.

## 7.0 Conclusions

The True Time Delay program (Low-Loss Fiber-Optic True Time Delay Generator for RF Signal Processing and Phased Array Antenna Control) has, over the last three years, developed the Fiber Bragg True Time Delay concept to a form that could be implemented into a phased array system. In addition, the True Time Delay Program has positioned us to develop a wide class of RF photonic signal processing structures.

During the course of the program we have proven our ability to make high quality fiber optic Bragg gratings, the key element in the True Time Delay concept. We can write gratings in 5 different types of fiber that are single mode at  $1.3\mu$  and  $1.5\mu$  with reflectivities of 100% and we can write gratings in planar silica waveguide material. We've achieved sidelobe suppression of 50 dBc at 2 nm channels and 60 dBc at 3 nm channels and gratings have been written in both polarization preserving fiber and non polarization preserving fibers. We have developed an analytical model to predict the performance characteristics of the gratings for any chirp and grating writing intensity profile. We have a wavelength positioning accuracy of 0.036 nm absolute and 0.01 nm relative. Our spatial positioning accuracy, which translates to time delay accuracy, is 2-3 picosecond, with 28 picosecond verified. We have designed and fabricated a TTD package that contains a 16 grating, 4-bit, time delay element with an optical circulator in a compact, somewhat rugged package.

## ***MISSION OF ROME LABORATORY***

Mission. The mission of Rome Laboratory is to advance the science and technologies of command, control, communications and intelligence and to transition them into systems to meet customer needs. To achieve this, Rome Lab:

- a. Conducts vigorous research, development and test programs in all applicable technologies;
- b. Transitions technology to current and future systems to improve operational capability, readiness, and supportability;
- c. Provides a full range of technical support to Air Force Material Command product centers and other Air Force organizations;
- d. Promotes transfer of technology to the private sector;
- e. Maintains leading edge technological expertise in the areas of surveillance, communications, command and control, intelligence, reliability science, electro-magnetic technology, photonics, signal processing, and computational science.

The thrust areas of technical competence include: Surveillance, Communications, Command and Control, Intelligence, Signal Processing, Computer Science and Technology, Electromagnetic Technology, Photonics and Reliability Sciences.